Petroleum Science 23 (2026) 4559–4576

Contents lists available at ScienceDirect

Petroleum Science

journal homepage: www.keaipublishing.com/en/journals/petroleum-science

Original Paper

In-situ stress controlled reservoir quality in ultra-deep sandstones in Qiulitage Structural Belt, Kuqa Depression, Tarim Basin, NW China

Lu Xiao [a,b], Jin Lai [a,b,*], Xun Yang [a,b], Fei Zhao [a,b], Dong Li [c], Hong-Bin Li [a,b], Yong-Ping Wu [d], Bo Zhu [d], Gui-Wen Wang [a,b]

[a] State Key Laboratory of Petroleum Resources and Engineering, China University of Petroleum (Beijing), Beijing, 102249, China
[b] College of Geosciences, China University of Petroleum (Beijing), Beijing, 102249, China
[c] Xinjiang Research Institute of the Huairou Laboratory, Urumqi, 830011, Xinjiang, China
[d] Research Institute of Petroleum Exploration and Development, Tarim Oilfield Company, CNPC, Korla, 841000, Xinjiang, China

ARTICLE INFO

Article history:
Received 20 August 2025
Received in revised form
5 January 2026
Accepted 22 May 2026
Available online 28 May 2026

Edited by Xiu-Fang Hu

Keywords:
Kuqa Depression
Ultra-deep reservoir
In-situ stress
Reservoir quality
Well logs

ABSTRACT

High industrial natural flow has been produced from the ultra-deep Cretaceous Bashijiqike sandstones (>6000 m) in the Qiulitage Structural Belt in the Kuqa Depression, Tarim Basin, northwestern China. However, the Cretaceous Bashijiqike reservoirs exhibit strong heterogeneity and significant reservoir quality variations. The complex in-situ stress state plays a critical role in reservoir quality; however, little research has been performed on the relationship between in-situ stress and reservoir quality, which constrains efficient hydrocarbon exploration and development. In order to clarify the in-situ stress-controlled reservoir quality variations, cores, thin sections and well log data are integrated to clarify the depositional microfacies, diagenesis and in-situ stress. The in-situ stress orientation and magnitude characteristics are investigated, and the distribution patterns of stress state are analyzed considering sedimentary environments and diagenesis. The results show that in-situ stress in Zhongqiu 1 gas field of Qiulitage Structural Belt remains unreleased since rare fractures are formed, and horizontal stress differences are greatly varied due to structural patterns, lithology assemblages and variations of geomechanical properties. The current maximum principal stress (S_{hmax}) orientation is NW–SE, derived by image logs in the Cretaceous Bashijiqike reservoirs of Zhongqiu 1 gas field. Vertical stress (S_v) is determined by integrating bulk density of the overburden rocks, while the maximum horizontal principal stress (S_{hmax}) and the minimum horizontal principal stress (S_{hmin}) are calculated by the combined spring model using density and sonic logs. A significant negative correlation relationship is observed between measured porosity and horizontal in-situ stress differences ($\Delta\sigma = S_{hmax} - S_{hmin}$). The measured helium porosity is reduced to 9.4% when the $\Delta\sigma$ is higher than 40 MPa. Intensive stress compression will contribute to a high compactional porosity loss (COPL), and COPL reaches 34.2% when the $\Delta\sigma$ becomes higher than 40 MPa. Layers with lower $\Delta\sigma$ values exhibit higher reservoir porosity and also higher natural gas production. Overall, favorable reservoirs are distributed at the center of sandbody in underwater distributary channel microfacies, and the sandstones are fine- to medium-grained and well-sorted with low in-situ stress differences. In-situ stress will control the compaction behaviors and the matrix porosity of sandstones, and also determines the hydrocarbon productivity. The results will provide insights into the reservoir quality variations in ultra-deep sandstones, and have implications for deep buried rocks with complex stress conditions worldwide.

1. Introduction

With the advancement of theory and technology, the focus of oil and gas exploration has shifted from shallow to deep and ultra-deep strata, leading to significant discoveries of petroleum and gas in deep (4500–6000 m) to ultra-deep (>6000 m) reservoirs (Lai et al., 2023; Laubach et al., 2023; Xu et al., 2025). The Tarim

* Corresponding author.
E-mail address: laijin@cup.edu.cn (J. Lai).
Peer review under the responsibility of China University of Petroleum (Beijing).

https://doi.org/10.1016/j.petsci.2026.05.039

Basin, as one of the richest basins in ultra-deep oil and gas globally, is a key exploration target (Lai et al., 2017a; Guo et al., 2019). The Cretaceous Bashijiqike Formation in the Kuqa Depression of Tarim Basin is deeply buried; however, a series of giant gas fields with reserves over 1000×10^8 m^3 have been found in the Kuqa Depression, including the Kela 2, Keshen, Bozi-Dabei and Zhongqiu 1 gas fields (Lai et al., 2015, 2017b; Liu et al., 2019; Li et al., 2020, 2025; Xu et al., 2022a). At such depths, overburden pressure on the rock can surpass 140 MPa, with horizontal bidirectional stress differences reaching 50 MPa (Ferraro et al., 2019; Zeng et al., 2020a). These ultra-deep reservoirs display strong heterogeneity due to intense stress caused by ultra-deep burial (Matonti et al., 2017; Sun et al., 2017; Lai et al., 2019). In addition, the gas wells show enormous productivity variations even within the same structural environment (Vandeginste et al., 2012; Lai et al., 2023). Reservoir quality in ultra-deep sandstones is heavily influenced by in-situ stress state, and the in-situ stress controls fracture effectiveness, and also determines compaction behaviors and thus matrix porosity (Sun et al., 2017; Del Sole et al., 2020; Zeng et al., 2020a, 2020b; de Souza Rodrigues et al., 2021). Intensive paleostress will result in the formation of natural fractures, and fractures are an important factor improving permeability and hydrocarbon flows, while weak in-situ stress helps preserve primary pores and improve pore connectivity (Lin et al., 2023; Ning et al., 2024; Tan et al., 2024; Li et al., 2025; Tian et al., 2025). Currently, there are various methods for in-situ stress measurement, including hydraulic fracturing tests and acoustic emission experiments (Zoback et al., 1993; Lai et al., 2019; Zhang et al., 2022, 2024a; Akkiraju et al., 2025; Sun et al., 2025).

Large-scale faults and fractures are commonly developed in ultra-deep and high-pressure conditions, and these faults and fractures will significantly enhance reservoir properties and hydrocarbon productivity (Lai et al., 2023). However, no large-scale fractures are detected in the Qiulitage Structural Belt in the Kuqa Depression, and the strong stress is therefore not released (Zeng et al., 2010; Lai et al., 2026). Consequently, reservoirs show extremely heterogeneous performances due to the complex stress state. In the Zhongqiu 1 gas field, the daily natural gas flow of Well ZQ1 is 232×10^4 m^3, while that of the Well ZQ102 is only 7×10^4 m^3 (Li et al., 2020). Reservoir quality and natural gas productivity vary greatly in the same structural belt. Conventionally, sedimentation and diagenesis are considered the primary controls on reservoir quality (Bjørlykke, 2014; Haile et al., 2018; Lai et al., 2018a, 2023). Nevertheless, reservoir evaluation should account for in-situ stress in ultra-deep sandstone reservoirs, as stress critically controls reservoir properties (Ferraro et al., 2019; Del Sole et al., 2020; Wei et al., 2022; Xu et al., 2022a; Shi et al., 2024; Wang et al., 2025).

To improve the understanding of reservoir quality prediction using in-situ stress, image logs are employed to identify the orientations of S_{hmax}, while density and sonic well logs are utilized to calculate the magnitudes of S_{v}, S_{hmax}, and S_{hmin}. Relationships between in-situ stress and reservoir properties as well as gas productivity are analyzed by comparing stress magnitudes with porosity and oil test data, respectively. Under high-stress conditions, how in-situ stress controls reservoir quality is clarified by integrating depositional facies and diagenetic modification. The results on the relationships between in-situ stress magnitudes and reservoir quality of ultra-deep sandstones in Kuqa Depression will have implications for the ultra-deep hydrocarbon exploration in similar basins worldwide.

2. Geological setting

The Kuqa Depression is located at the northernmost part of the Tarim Basin, with the Tianshan Mountains' southern edge directly to its north (Zeng et al., 2010; Teng et al., 2020; Su et al., 2024, 2026; Zhao et al., 2025). The Kuqa Depression is a foreland depression in the southern Tianshan Mountains piedmont, consisting of Meso-Cenozoic sediments (Shi et al., 2004). Controlled by the India-Asia plate collision, the depression has experienced compression, extension, and rejuvenated foreland basin stages since the Permian. During its evolution, numerous thrust faults and folds have been formed. The depression exhibits a "four belts and three sags" structural pattern. The four belts (north to south): the Northern Monocline Belt, the Kelasu and Qiulitage structural belts, and the Southern Gentle Monocline Belt. The three sags (west to east): Wushi Sag, Baicheng Sag, and Yangxia Sag (Fig. 1) (Feng et al., 2018; Ju and Wang, 2018). The Qiulitage Structural Belt is subdivided into four segments (west to east): Jiamu, Xiqiu, Zhongqiu and Dongqiu blocks, with the Zhongqiu Block representing its central section (Fig. 1) (Zeng et al., 2010; Lai et al., 2017b).

The Cretaceous Bashijiqike Formation (K_1bs) is one of the main exploration targets in the Zhongqiu 1 gas field of Qiulitage Structural Belt. The Bashijiqike Formation in the Qiulitage Structural Belt exceeds 6000 m in burial depth and 200 m in thickness. During the Late Cretaceous, the Upper Cretaceous deposits in the Kuqa Depression were completely eroded, and only the Lower Cretaceous were left (Li et al., 2020). The K_1bs is overlain by the Paleogene Kumugeliemu Group, which is a set of massive gypsum-salt rock strata exhibiting excellent caprock properties. The source rocks for the K_1bs reservoir are mainly the underlying coal-bearing strata, including the Jurassic Yangxia Formation (J_1y), Triassic Karamay Formation (T_2k), and Huangshanjie Formation (T_3h) (Lai et al., 2022).

In the Kuqa Depression, the Bashijiqike Formation is divided into three members (from top to bottom): the First Member (K_1bs^1), Second Member (K_1bs^2), and Third Member (K_1bs^3) (Li et al., 2020). Both K_1bs^1 and K_1bs^2 consist of braided river delta front deposits, while K_1bs^3 comprises fan delta front deposits. These units feature underwater distributary channel microfacies, interdistributary bay microfacies, and mouth bar microfacies. The lithology is predominantly fine- to medium-grained lithic feldspar sandstone. Reservoir spaces include primary intergranular pores and a few intergranular and intragranular dissolution pores (Lai et al., 2017b; Li et al., 2020; Xu et al., 2022a).

3. Samples and methods

3.1. Samples

Core samples are from two vertical wells (ZQ101 and ZQ102) in the Zhongqiu 1 gas field of Qiulitage Structural Belt, and a total of 45 m of cores from the Bashijiqike Formation are collected. In addition, cores are slabbed 360° to better document sedimentary and structural characteristics. Core plug samples are prepared for thin section analysis.

Helium porosity and permeability have been measured in 242 core plug samples. These thin sections are impregnated with blue-dye resin to highlight pore systems. Thin sections are also used to detect depositional composition and texture (including grain size and sorting).

Scanning electron microscope (SEM) secondary electron image analysis can be conducted to show authigenic clay minerals and pore-filling cements (mainly quartz and calcite cements), and the pore throat spaces can also be recognized.

Conventional well logs contain two lithology logs (natural gamma ray (GR) and calipers (CAL)), triple porosity logs (bulk density (DEN), compressional wave slowness (DTC) and compensated neutron log (CNC)), and high-resolution induction resistivity

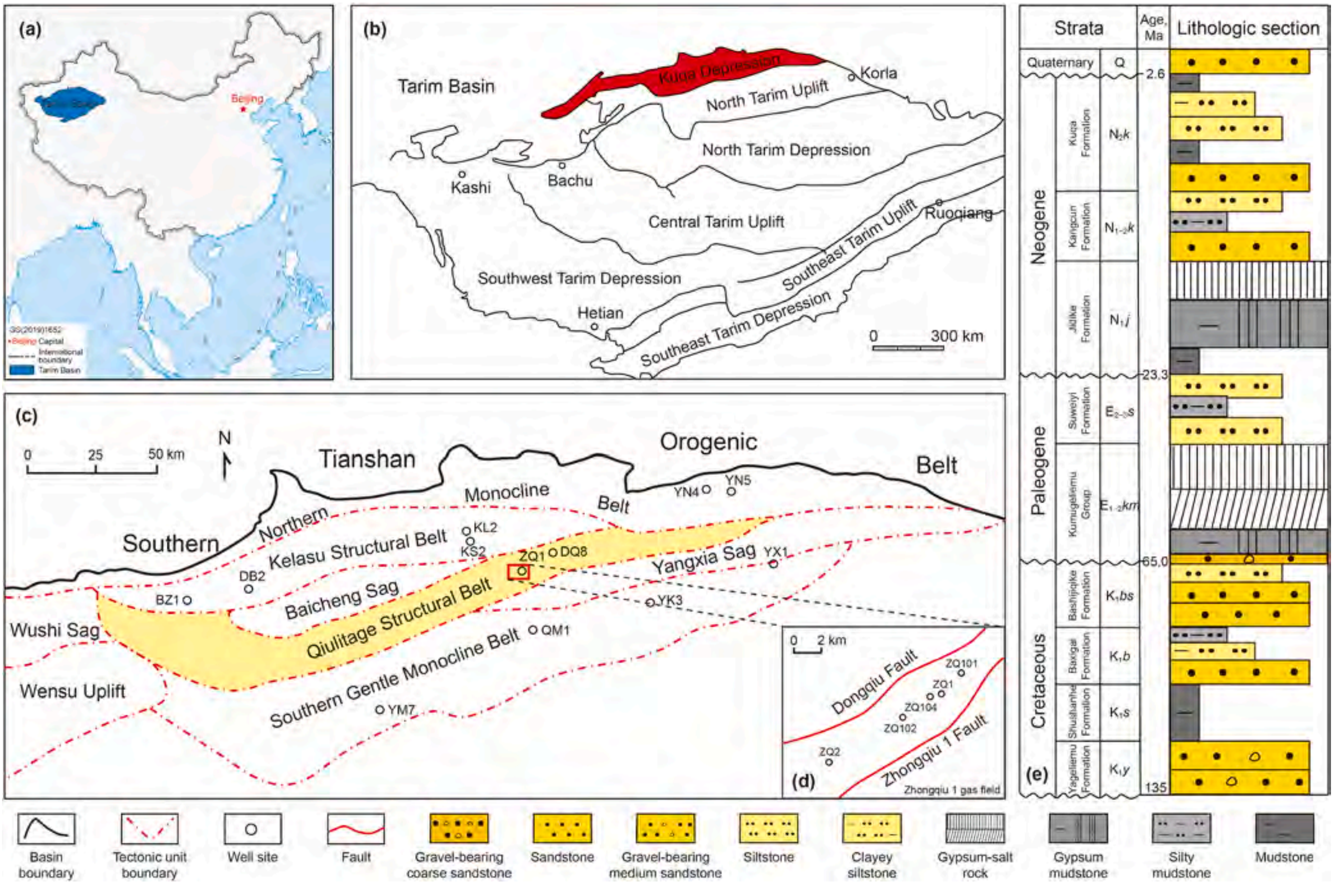

Fig. 1. **(a)** Location of the Tarim Basin in China; **(b)** distribution map of the Kuqa Depression within the northern Tarim Basin; **(c)** map showing the structural division of the Kuqa Depression and location of Qiulitage Structural Belt in the Kuqa Depression (Lai et al., 2023); **(d)** well location map of Zhongqiu 1 gas field in Qiulitage Structural Belt; **(e)** stratigraphic column of the Qiulitage Structural Belt in the Kuqa Depression (Liu et al., 2019).

logs (M2R1, M2R3, M2R*x*, etc.). Moreover, the calculated porosity is derived from the triple porosity curves in this study.

Baker Hughes Company's EI (Earth Imager) image logs can generate the high-resolution (vertical resolution: 0.3 inch) borehole images. The image logs are run in oil-based drilling mud which is non-conductive. After static and dynamic correction/normalization, the raw data are converted to geological features (such as beddings, fractures) for manual identification and interpretation (Fernández-Ibáñez et al., 2018; Lai et al., 2018b).

Atlas's XMAC is one type of full-waveform data captured by multipole array acoustic tools (Li et al., 2022; Huang et al., 2025). In the following sections, the XMAC logging tools are used to extract shear slowness (DTS), which can be used to calculate geomechanical parameters (Poisson's ratio and Young's modulus) (Xiang et al., 2015).

3.2. Theory and methods

Typically, the in-situ stress orientation can be derived from image logs (Rajabi et al., 2010; Wilson et al., 2015; Huffman and Saffer, 2016; Mafakheri Bashmagh et al., 2024; Cao et al., 2025). The in-situ stress orientation is determined by detecting induced fractures and borehole breakouts formed during drilling, as identified by image logs (Song and Haimson, 1997; Zoback et al., 2003; Huffman and Saffer, 2016; Kingdon et al., 2016; Najibi et al., 2017; Ning et al., 2024). After wellbore formation, the original in-situ stress equilibrium is disrupted, causing stress redistribution around the wellbore and possibly resulting in observable borehole breakout phenomena. According to elastic mechanics theory, the long axis of the elliptical borehole caused by stress collapse indicates the S_{hmin} direction (Bell and Gough, 1979; Rajabi et al., 2010; Massiot et al., 2015; Lai et al., 2018b). Meanwhile, it is most prone to form tensile fractures along the direction of S_{hmax} where effective axial stress is minimal, forming induced fractures around the wellbore wall (Tingay et al., 2011; Nian et al., 2016). Thus, the induced fractures can indicate the direction of S_{hmax} (Lai et al., 2017a, 2019).

Anderson (1951) classifies the stress regimes according to the relative magnitudes of S_{hmax}, S_{hmin} and S_{v}: (1) Normal faulting stress regime: $S_{\mathrm{v}} > S_{\mathrm{hmax}} > S_{\mathrm{hmin}}$; (2) Strike-slip faulting stress regime: $S_{\mathrm{hmax}} > S_{\mathrm{v}} > S_{\mathrm{hmin}}$; (3) Reverse-faulting stress regime: $S_{\mathrm{hmax}} > S_{\mathrm{hmin}} > S_{\mathrm{v}}$ (Xu et al., 2022a; Zhang et al., 2022).

In-situ stress magnitude (S_{hmax}, S_{hmin} and S_{v}) can be determined by constructing the 1-D MEMs (one-dimensional mechanical Earth models) (Tingay et al., 2009; Lai et al., 2024). At a specific depth, S_{v} magnitude is determined by overburden pressure from the overlying rocks and pore fluids. Therefore, it is conventionally derived by integrating the bulk density of the overburden from the surface to the specified depth (Eq. (1)) (Maleki et al., 2014).

$$S_{\mathrm{v}} = \int_0^z \rho g \mathrm{d}z \tag{1}$$

where, ρ is the bulk density from DEN logs, kg/m^3; g is the gravitational acceleration, m/s^2; z is the burial depth, m; S_{v} is the vertical stress, MPa (Verweij et al., 2016; Zhang and Zhang, 2017; Lai et al., 2019).

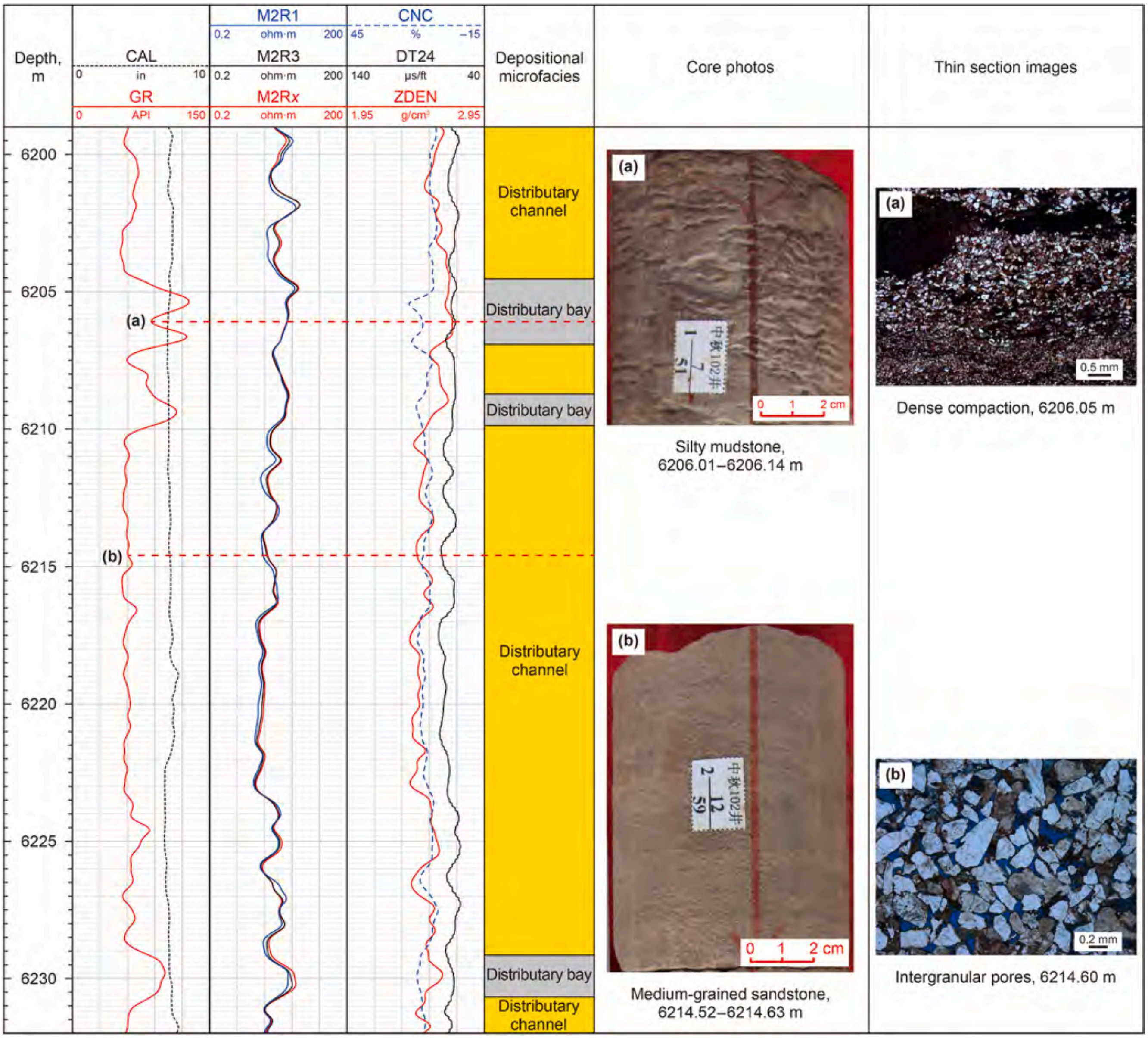

Fig. 2. Conventional logging response and core and thin section characteristics of the underwater distributary channel and interdistributary bay microfacies of Bashijiqike Formation in the Zhongqiu 1 gas field of the Kuqa Depression.

Pore pressure (P_p) is the in-situ pore fluid pressure within the pores at a given depth (Najibi et al., 2017; Shi et al., 2024). Eaton (1969) introduced a method to estimate pore pressure using sonic well logs (Eq. (2)) (Zhang, 2011; Lai et al., 2019).

$$P_p = P_o - (P_o - P_w)\left(\frac{\Delta t_n}{\Delta t_p}\right)^c \tag{2}$$

where, P_o is the overburden stress (S_v), MPa; P_p is the pore pressure, MPa; P_w is the hydrostatic pressure (9.8 MPa/km for simplification), MPa; Δt_n is the sonic interval transit time at the normal pressure, μs/ft; Δt_p is the compressional wave slowness (DTC), μs/ft; and c is the coefficient of compaction (Ju et al., 2017; Lai et al., 2019).

The dynamic Young's modulus (E_d) and dynamic Poisson's ratio (ν_d) are two key parameters for the calculation of in-situ stress. The methods of calculating these two parameters using well log data are as follows (Eqs. (3) and (4)) (Xu et al., 2022a):

$$E_d = \frac{\rho_b}{\Delta t_s^2} \cdot \frac{3\Delta t_s^2 - 4\Delta t_p^2}{\Delta t_s^2 - \Delta t_p^2} \tag{3}$$

$$\nu_d = \frac{\Delta t_s^2 - 2\Delta t_p^2}{2\left(\Delta t_s^2 - \Delta t_p^2\right)} \tag{4}$$

where, ρ_b is rock density, kg/m^3; Δt_p is the compressional wave slowness, μs/ft; Δt_s is shear slowness, μs/ft.

Multiple in-situ stress calculation models have been put forward to determine the magnitude of the three types of stress (S_v, S_{hmax} and S_{hmin}). The calculation of S_v is generally undisputed. But for calculation of the horizontal principal stress magnitudes, a

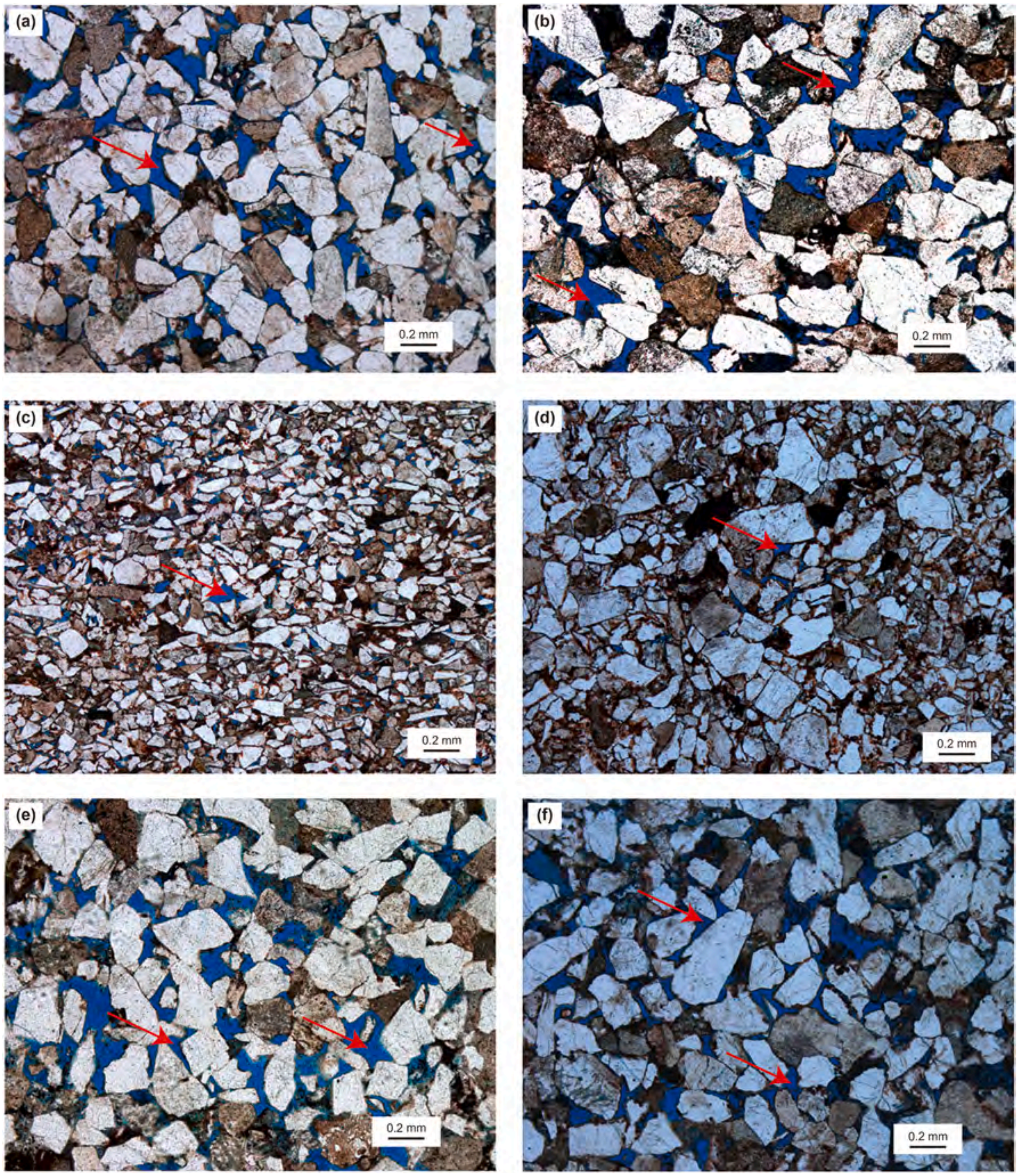

Fig. 3. Thin section images (pore space is shown in blue) under polarized light microscopes showing the diagenesis of the Bashijiqike Formation in Zhongqiu 1 gas field of Kuqa Depression: **(a)** moderate degree of compaction, abundance of primary intergranular pores (with grain-coating clays) (red arrows), Well ZQ102, 6393.50 m; **(b)** moderate degree of compaction, abundance of primary intergranular pores (with grain-coating clays) (red arrows), Well ZQ101, 6300.66 m; **(c)** extensive compaction and minor pores (red arrow), Well ZQ102, 6219.49 m; **(d)** high degree of compaction, poor sorting and minor pores (red arrow), Well ZQ102, 6207.42 m; **(e)** moderate degree of compaction, abundance of primary intergranular pores (with grain-coating clays) (red arrows), rare dissolution pores, Well ZQ101, 6286.58 m; **(f)** moderate degree of compaction, abundance of primary intergranular pores (with grain-coating clays) (red arrows), rare dissolution pores, Well ZQ102, 6214.60 m.

large number of calculation models exist, including the biaxial strain model, combined spring model, Huang's model, Coulomb Navier failure model, Mohr Coulomb failure model, uniaxial strain model, etc. (Rasouli and Sutherland, 2014; Xu et al., 2022a).

The Kuqa Depression has experienced multistage tectonic evolution, and the horizontal tectonic stress is strong, and therefore the combined spring model has been optimized by many scholars for the calculation of three stress magnitudes for the Kuqa Depression (Xu et al., 2022a; Lai et al., 2024; Zhang et al., 2024b). In this model, the S_{hmax} and S_{hmin} magnitudes are calculated according to Poisson's ratio, Young's modulus, pore pressure and vertical stress (Eqs. (5) and (6)). $\Delta\sigma$ is the difference between S_{hmax} and S_{hmin} (Eq. (7)) (Eaton, 1969; Thiercelin and Plumb, 1994; Yeltsov et al., 2014; Radwan and Sen, 2021).

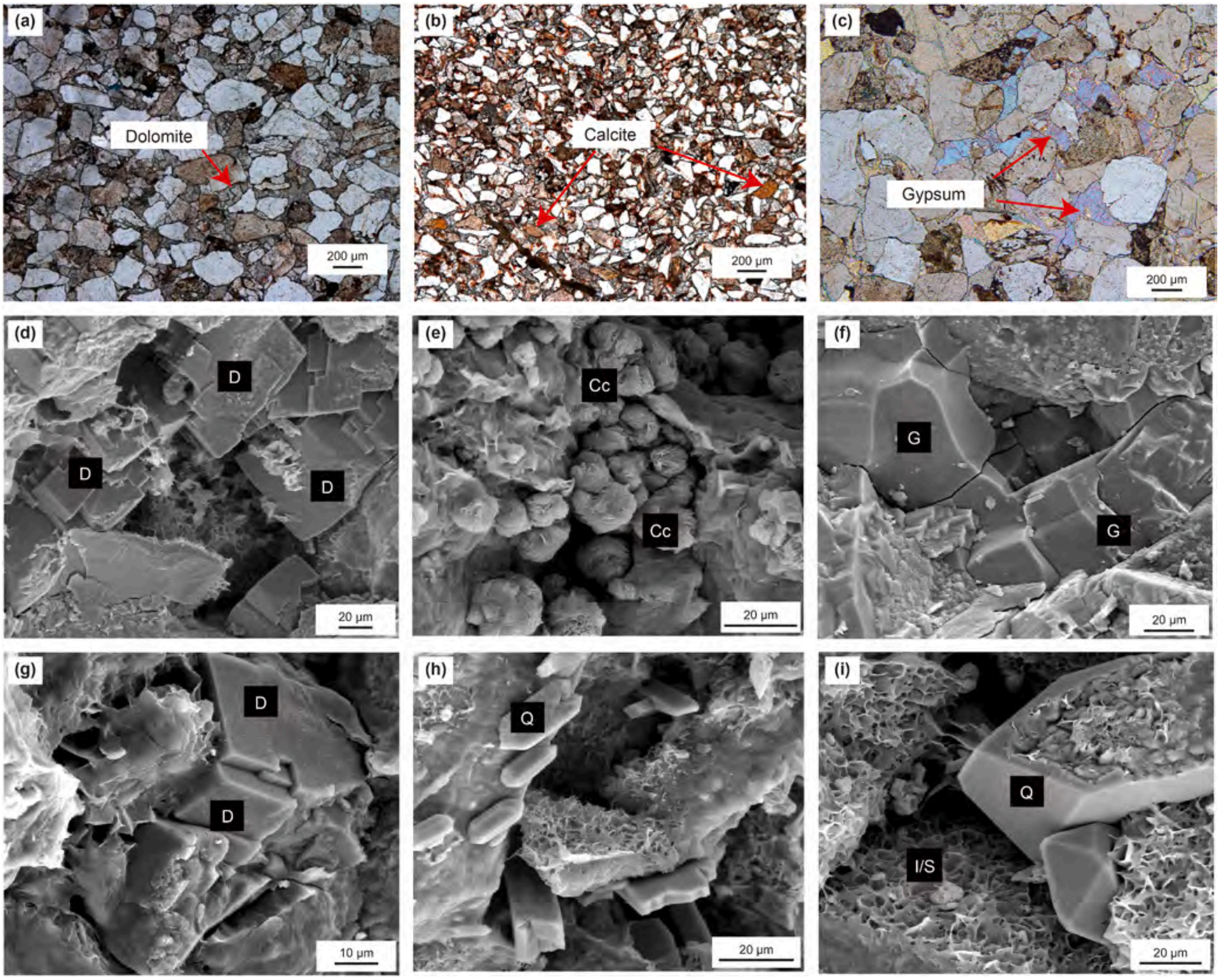

Fig. 4. Photomicrographs showing diagenetic minerals of the Bashijiqike Formation in Zhongqiu 1 gas field of Kuqa Depression: **(a)** dolomite cements filling in the pore spaces, Well ZQ101, 6298.73 m; **(b)** calcite cements filling in the pore spaces, Well ZQ101, 6290.23 m; **(c)** gypsum cements filling in the pore spaces, Well ZQ101, 6298.11 m; **(d)** D = dolomite cements, Well ZQ101, 6338.77 m; **(e)** Cc = calcite cements, Well ZQ101, 6299.43 m; **(f)** G = gypsum cements, Well ZQ101, 6298.11 m; **(g)** D = dolomite cements, Well ZQ101, 6337.01 m; **(h)** Q = quartz, minor amount of quartz cements, Well ZQ101, 6335.97 m; **(i)** I/S = mixed layered illite/smectite, Well ZQ101, 6301.42 m.

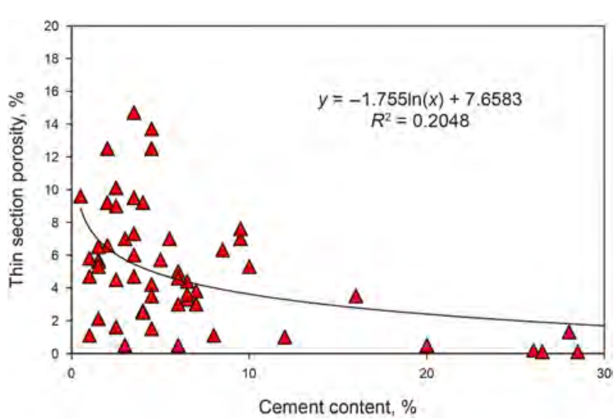

Fig. 5. Comparisons of cement content and thin section porosity of the Bashijiqike Formation in Zhongqiu 1 gas field of Kuqa Depression.

$$S_{\text{hmax}} = \frac{\nu}{1-\nu}S_{\text{v}} - \frac{\nu}{1-\nu}\alpha P_{\text{p}} + \alpha P_{\text{p}} + \frac{E}{1-\nu^2}\varepsilon_{\text{H}} + \frac{\nu E}{1-\nu^2}\varepsilon_{\text{h}} \tag{5}$$

$$S_{\text{hmin}} = \frac{\nu}{1-\nu}S_{\text{v}} - \frac{\nu}{1-\nu}\alpha P_{\text{p}} + \alpha P_{\text{p}} + \frac{E}{1-\nu^2}\varepsilon_{\text{h}} + \frac{\nu E}{1-\nu^2}\varepsilon_{\text{H}} \tag{6}$$

$$\Delta\sigma = S_{\text{hmax}} - S_{\text{hmin}} \tag{7}$$

where, α is the Biot coefficient, dimensionless, which can be obtained on empirical equation (Eq. (8)); E is the Young's modulus, GPa; ν is Poisson's ratio, dimensionless; ε_{H} and ε_{h} are strain in S_{hmax} and S_{hmin} directions respectively as given by Eqs. (9) and (10), dimensionless; P_{p} is the pore pressure, MPa; S_{hmax} and S_{hmin} is the maximum and minimum horizontal principal stress, respectively, MPa; S_{v} is the vertical principal stress, MPa (Maleki et al., 2014; Kidambi and Kumar, 2016; Najibi et al., 2017; Zhang et al., 2024c).

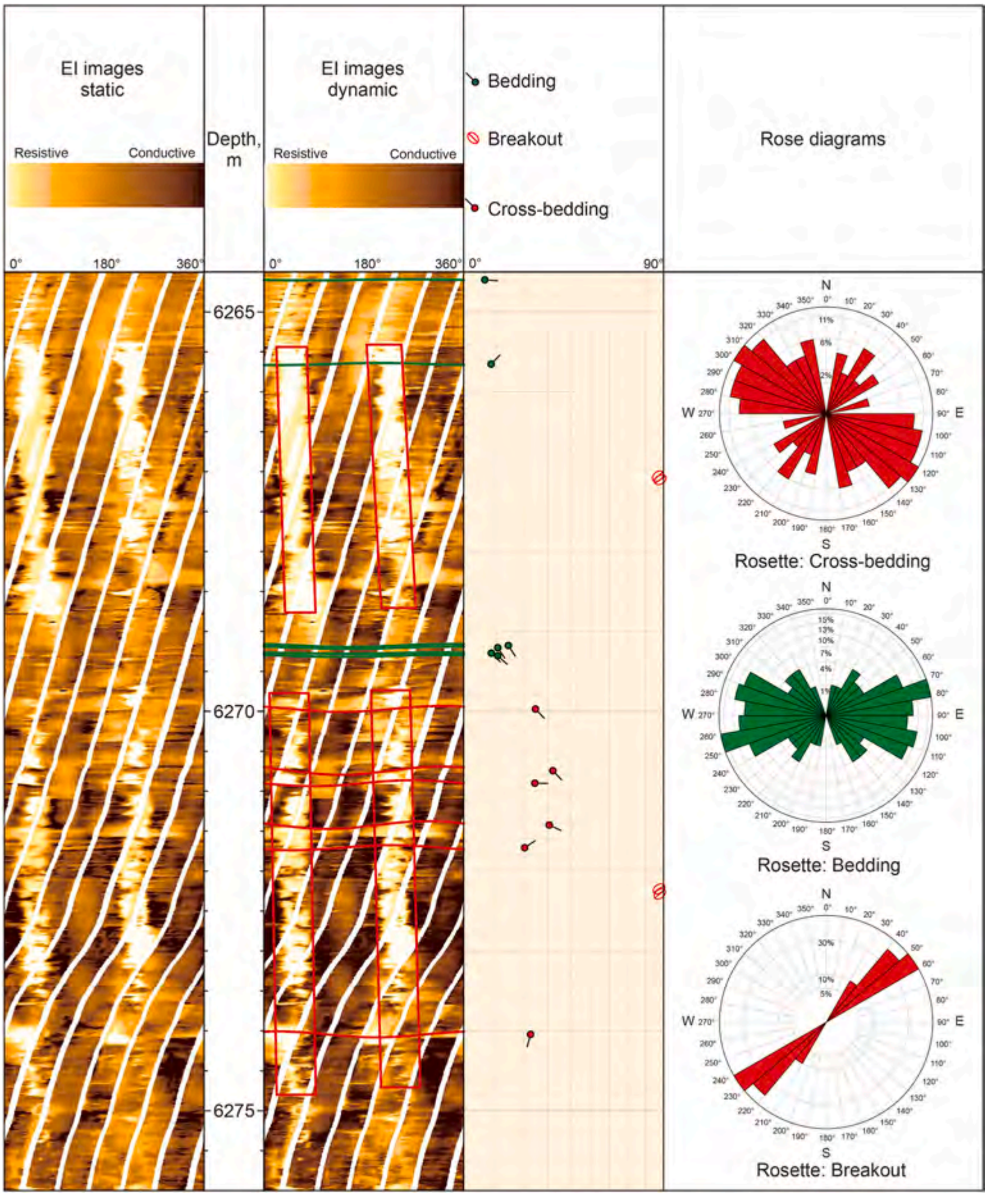

Fig. 6. Bedding, cross-bedding, and borehole breakout interpreted from image logs in Well ZQ101 of Bashijiqike Formation in the Zhongqiu 1 gas field of the Kuqa Depression. Note that borehole breakouts are observed as interpreted bright bands on opposite sides of the borehole.

Table 1
The stress magnitude of Bashijiqike Formation in the Zhongqiu 1 gas field of the Kuqa Depression.

Well	S_{hmax}, MPa	S_{hmin}, MPa	$\Delta\sigma$, MPa
ZQ1	174.77	126.37	28.4
ZQ101	176.67	144.52	32.15
ZQ102	184.66	144.53	40.13
ZQ104	165.75	129.44	36.29

$$\alpha = 1 - \exp\left(7.5 \tan\frac{\varphi\pi}{2}\right) \tag{8}$$

$$\varepsilon_{\mathrm{h}} = \frac{S_{\mathrm{V}} \times \nu}{\mathrm{E}} \times \left(\frac{1}{1-\nu} - 1\right) \tag{9}$$

$$\varepsilon_{\mathrm{H}} = \frac{S_{\mathrm{V}} \times \nu}{\mathrm{E}} \times \left(1 - \frac{\nu^2}{1-\nu}\right) \tag{10}$$

where φ is the porosity derived from both laboratory tests and well logs (Binh et al., 2007).

4. Results

4.1. Depositional microfacies

In the Zhongqiu 1 gas field, the K_1bs^3 is deposited in a fan delta front sedimentary environment, while the depositional facies of K_1bs^2 and K_1bs^1 are braided river delta front facies (Liu et al., 2019; Li et al., 2020; Zhu et al., 2023). Sandbodies in the Bashijiqike Formation are mainly formed in underwater distributary channel

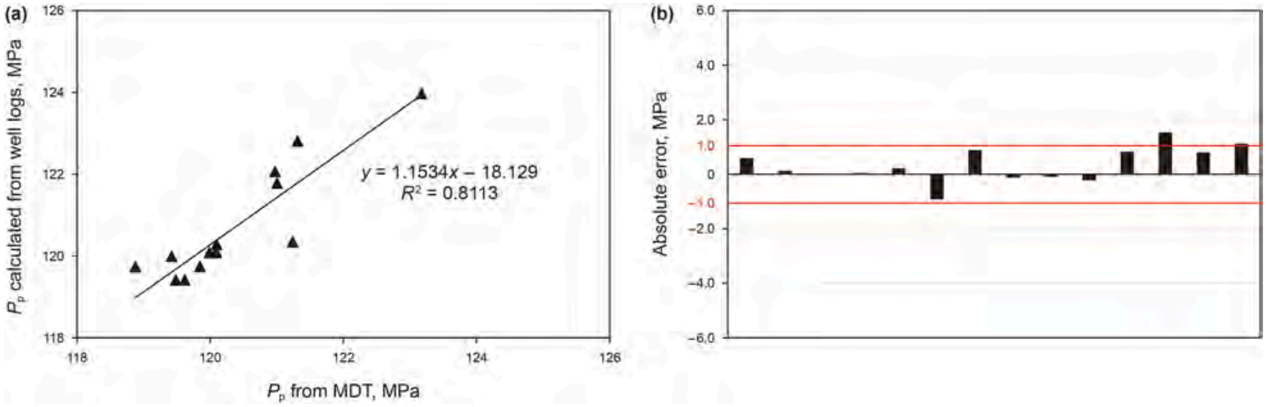

Fig. 7. (**a**) Comparisons of P_p derived from MDT experiment and calculated from well logs of the Bashijiqike Formation in Zhongqiu 1 gas field of Kuqa Depression; (**b**) error analysis of P_p of the Bashijiqike Formation in Zhongqiu 1 gas field of Kuqa Depression.

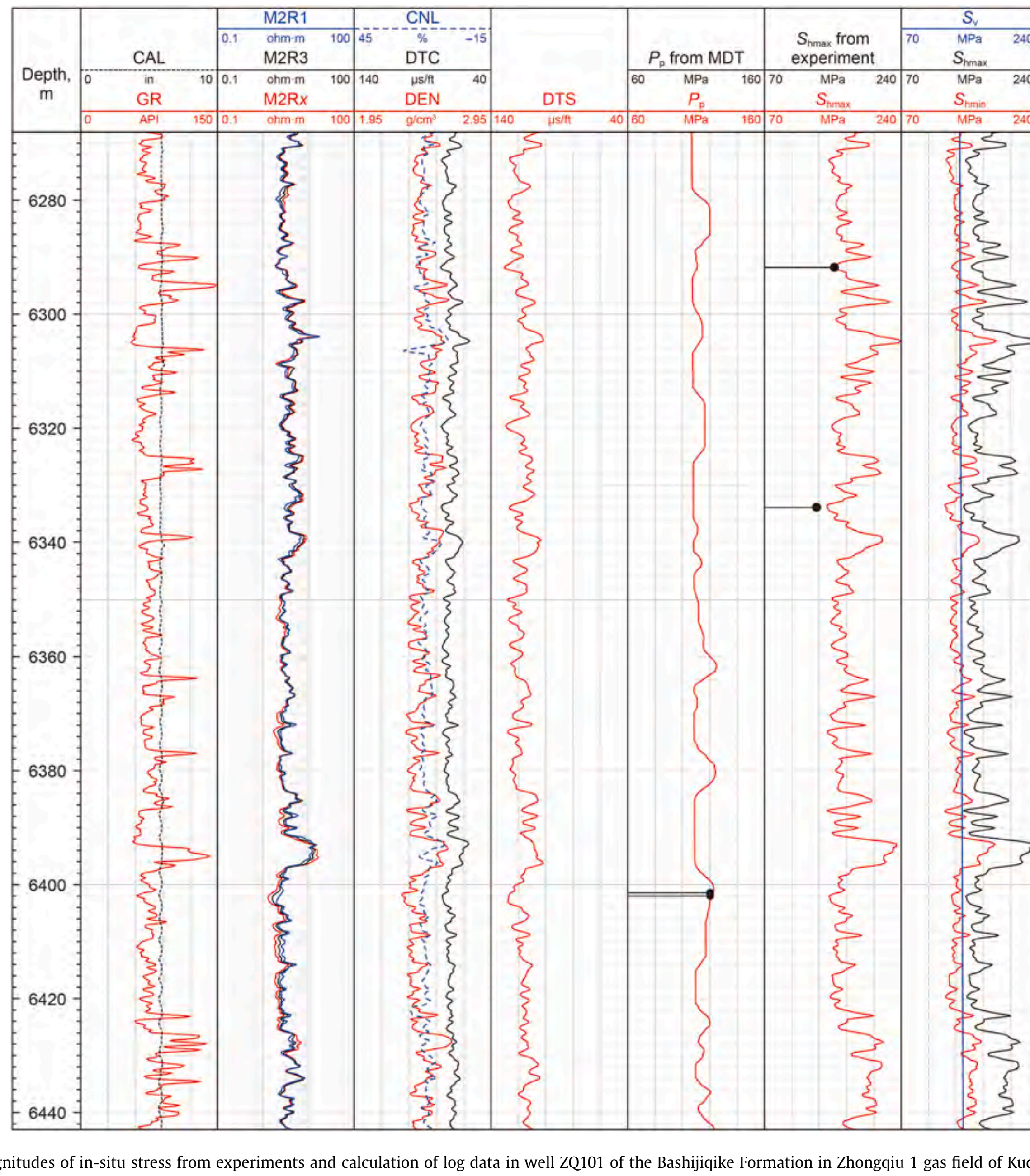

Fig. 8. Magnitudes of in-situ stress from experiments and calculation of log data in well ZQ101 of the Bashijiqike Formation in Zhongqiu 1 gas field of Kuqa Depression.

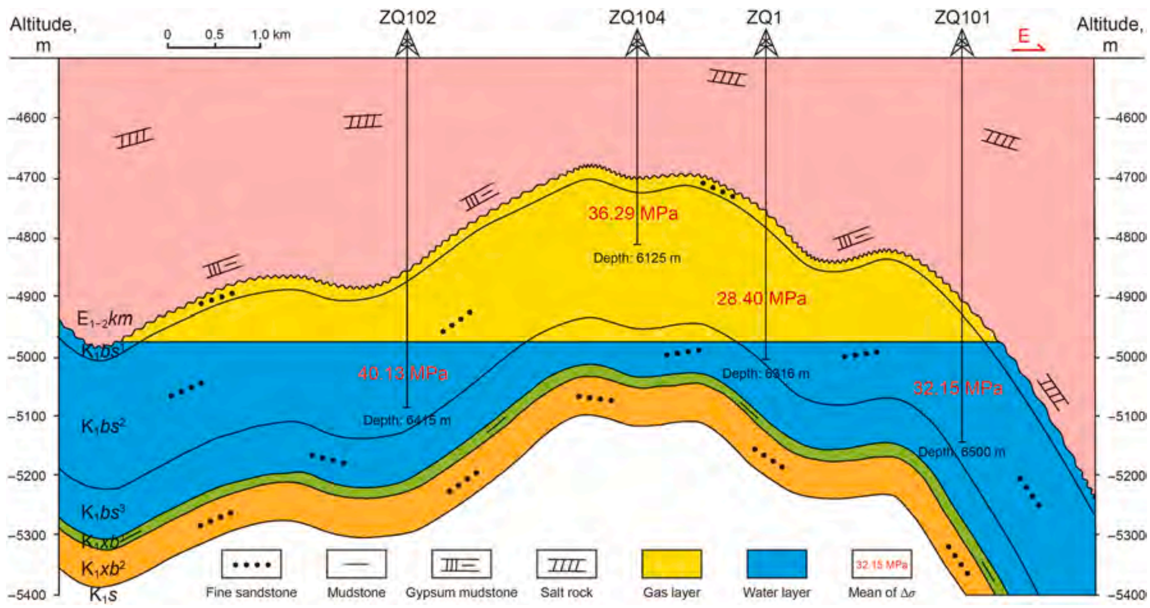

Fig. 9. Variations of in-situ stress magnitudes for the cross-section ZQ102–ZQ104–ZQ1–ZQ101 of Bashijiqike Formation in the Zhongqiu 1 gas field of the Kuqa Depression.

microfacies of delta front subfacies. The GR curve shows low values with a typical box-shaped pattern (Fig. 2). In contrast, the interdistributary bay microfacies are deposited in a weak sedimentary hydrodynamics. The GR curve displays high values with a typical finger-shaped pattern (Fig. 2). The lithology of Bashijiqike Formation is mainly brown, fine- to medium-grained sandstone, containing a small quantity of siltstone, argillaceous siltstone, and mudstone (Fig. 2).

4.2. Diagenesis

4.2.1. Diagenesis and pore spaces

In the Zhongqiu 1 gas field, the burial depth of the K_1bs exceeds 6000 m. Rocks have therefore experienced intensive compaction and cementation due to deep burial depths. However, widely developed primary intergranular pores are still commonly observed in the medium-grained sandstones, and point or point-to-line grain contacts are also detected (Fig. 3(a) and (b)). Few quartz cements are developed around the quartz grains, actually quartz cements are relatively rare in the Bashijiqike Formation based on optical microscope analysis (Fig. 3(a) and (b)). Rare intergranular pores are preserved in the very-fine-grained or poorly sorted rocks, and the grain contacts are mainly point to line (Fig. 3(c) and (d)). Thin section analysis reveals that primary intergranular pores are the predominant pore spaces in the Bashijiqike Formation (Fig. 3(e) and (f)), while dissolution pores are rarely developed (Fig. 3(e) and (f)). In addition, intergranular pores are only preserved in the medium-grained sandstones that are well sorted (Fig. 3(a), (b), (e) and (f)), while the fine- or very-fine-grained or the poorly sorted sandstones have no evident intergranular pore spaces (Fig. 3(c) and (d)).

4.2.2. Diagenetic minerals

Thin section and SEM image observations reveal that carbonate cements are the most pore-filling cements (Fig. 4). Dolomite (Fig. 4(a)), calcite (Fig. 4(b)) and gypsum (Fig. 4(c)) cements are detected by microscope and SEM analysis. Dolomite crystals are commonly detected filling the pore spaces (Fig. 4(g)). The calcite cements, which display a red color dyed by alizarin red S in thin sections, are commonly observed (Fig. 4(b)). Contiguous pore-filling gypsum can be observed in thin sections and SEM images (Fig. 4(c) and (f)). Quartz cement occurs in only minor amounts within pore spaces (Fig. 4(h)). In some cases, mixed layered illite/smectite is observed to inhibit the quartz cementation (Fig. 4(i)). Dolomite and gypsum constitute the volumetrically dominant diagenetic cements. Consequently, the presence of these cements greatly reduces thin section porosity, and when cement content exceeds 10%, porosity becomes less than 3.6% (Fig. 5).

4.3. In-situ stress direction and magnitude

As an intrinsic property of the Earth, in-situ stress can be described in terms of maximum principal horizontal stress (S_{hmax}), the minimum principal horizontal stress (S_{hmin}) and vertical principal stress (S_v) (Zoback et al., 2003; Tingay et al., 2009; Ju et al., 2017; Zhang et al., 2022; Lai et al., 2024).

4.3.1. In-situ stress direction

In the Kuqa Depression, analysis of image log data combined with the World Stress Map database indicates a predominant north-south orientation of S_{hmax} directions (Heidbach et al., 2010; Lai et al., 2019). Fig. 6 shows that the induced fractures of Well ZQ101 in the Kuqa Depression indicate a S_{hmax} direction of 210°–240°, and the perpendicular S_{hmin} direction is 120°–150° (Fig. 6).

4.3.2. In-situ stress magnitude

Calculated using the above formulas, the average values of stress magnitudes of S_{hmax}, S_{hmin}, S_v, and $\Delta\sigma$ of various wells in Zhongqiu 1 gas field are displayed in Table 1. The calculated P_p values show a high correlation with experimental values from MDT (Fig. 7(a)), and absolute error is mostly between −1 and 1 MPa (Fig. 7(b)). Meanwhile, the calculated S_{hmax} for Well ZQ101 matches well with experimental values (Fig. 8), demonstrating that the in-situ stress values derived from the model used in this study are accurate and reliable.

As shown in Fig. 9, the mean of $\Delta\sigma$ in ZQ104 (anticline hinge) is higher than the values in ZQ1 and ZQ101 (anticline limb). It reveals that strong stress has not been released by formation of natural fractures, therefore reservoir quality shows heterogeneous performances due to the complex stress state.

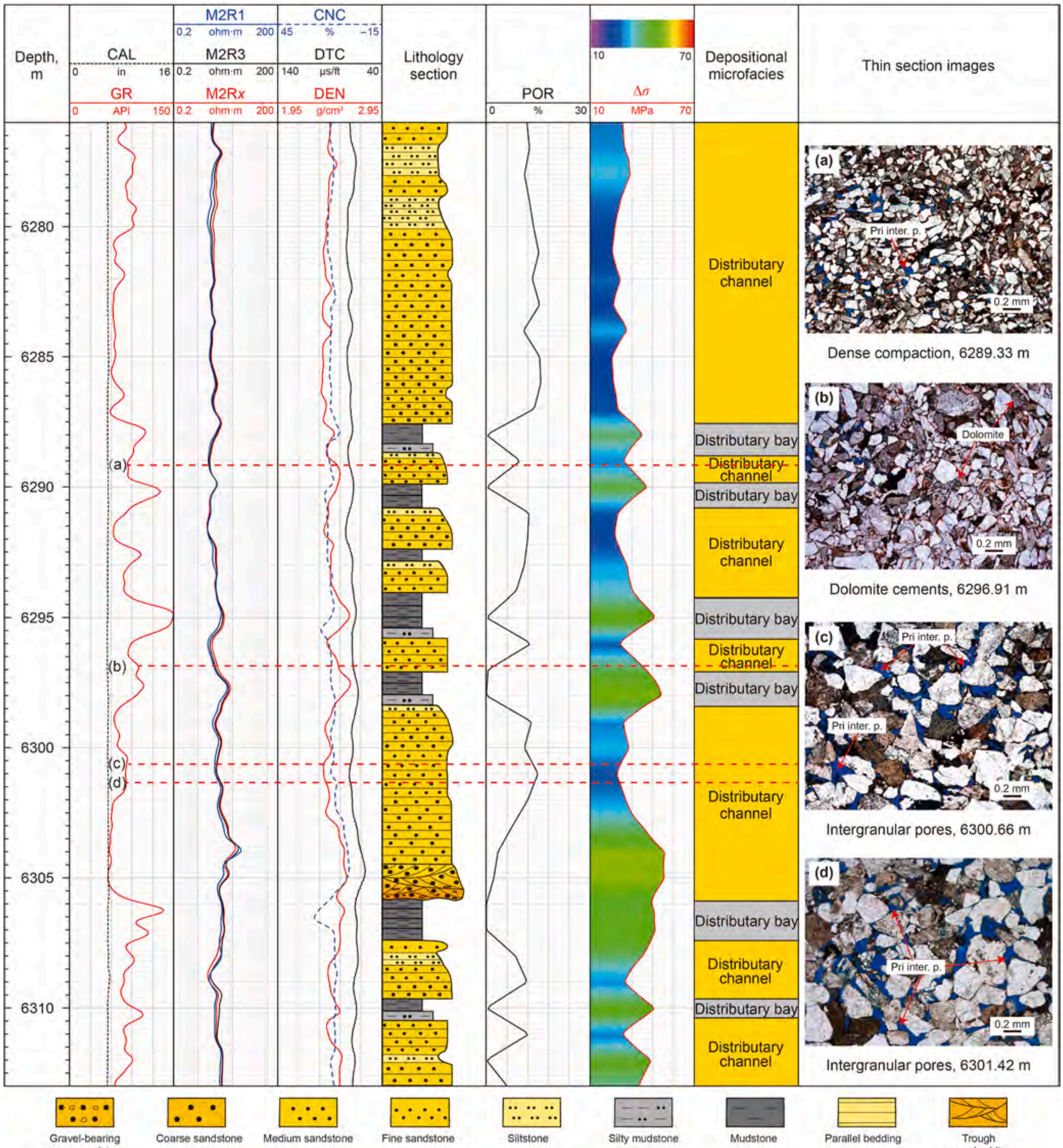

Fig. 10. Interpretation of depositional microfacies and in-situ stress for Well ZQ101 of Bashijiqike Formation in the Zhongqiu 1 gas field of the Kuqa Depression.

5. Discussion

5.1. Controls of depositional composition and texture on reservoir properties

Differences of sedimentary environments determine variations in the composition and texture of sediments (Fig. 2) (Morad et al., 2010; Taylor et al., 2010; Nguyen et al., 2013; Li et al., 2025). The texture and composition of sediments govern the reservoir's primary porosity (Bjørlykke, 2014).

The underwater distributary channel microfacies, which have box-shape and bell-shape GR curve shapes, are characterized by fining upward sequences or in some cases a unique sequence (no evident grain size change) (Fig. 10). At the top of the underwater distributary channel sandbody, the lithologies are mainly fine to very fine-grained sandstones, and these fine- to very-fine-grained and clay-rich sandstones are more likely to be tightly compacted (Fig. 10(a)). At the bottom of the sandbody, the sandstones are poorly sorted and more likely to be heavily cemented after the fluid squeezed out from the other side of the sand-mudstone

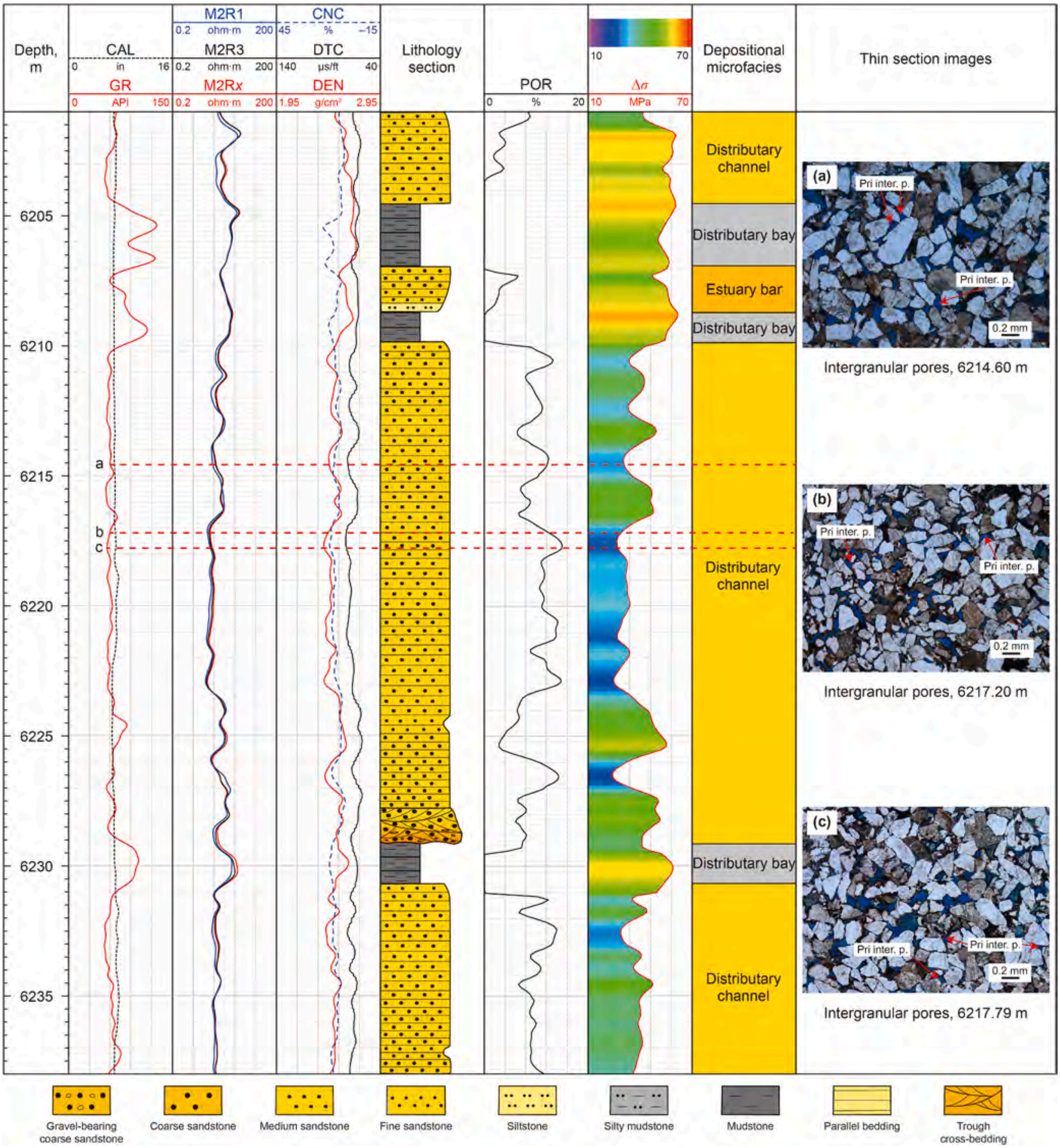

Fig. 11. Interpretation of depositional microfacies and in-situ stress for Well ZQ102 of Bashijiqike Formation in the Zhongqiu 1 gas field of the Kuqa Depression.

interface (Fig. 10(b)) (Milliken and Land, 1993; Dutton, 2008; Huang et al., 2021). Actually, carbonate cements can be commonly detected along the sandstone-mudstone contact surfaces (Mansurbeg et al., 2008). Therefore, the bottom and top parts of the underwater distributary channel sandbody have poor reservoir quality due to tight compaction and heavy cementation.

Conversely, in the center part of the underwater distributary channel sandbody, the lithologies are mainly fine- to medium-grained sandstones which are well sorted; consequently, mechanical compaction is limited and intergranular pores can be preserved (Fig. 10(c) and (d)). In addition, the center is far away from the sand-mudstone interface, therefore there is a poor condition for carbonate cementation (Fig. 10(c) and (d)). In Fig. 11, there is a nearly 20-m-thick underwater distributary channel sandbody, which has a bell-shape GR curve shape. In the center part of the sandbody, the lithologies are mainly fine-grained and well-sorted sandstones; consequently, intergranular pores can be preserved (Fig. 11(a)–(c)) (Bjørlykke, 1998; Thyne, 2001).

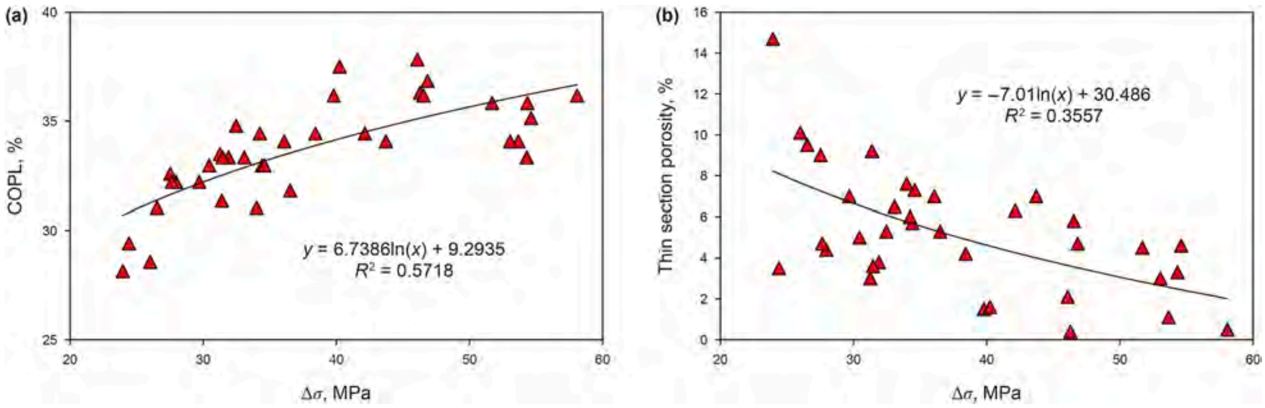

Fig. 12. **(a)** Scatter plot of horizontal in-situ stress difference and compactional porosity loss (COPL) of Bashijiqike Formation in the Zhongqiu 1 gas field of the Kuqa Depression; **(b)** scatter plot of horizontal in-situ stress difference and thin section porosity of Bashijiqike Formation in the Zhongqiu 1 gas field of the Kuqa Depression.

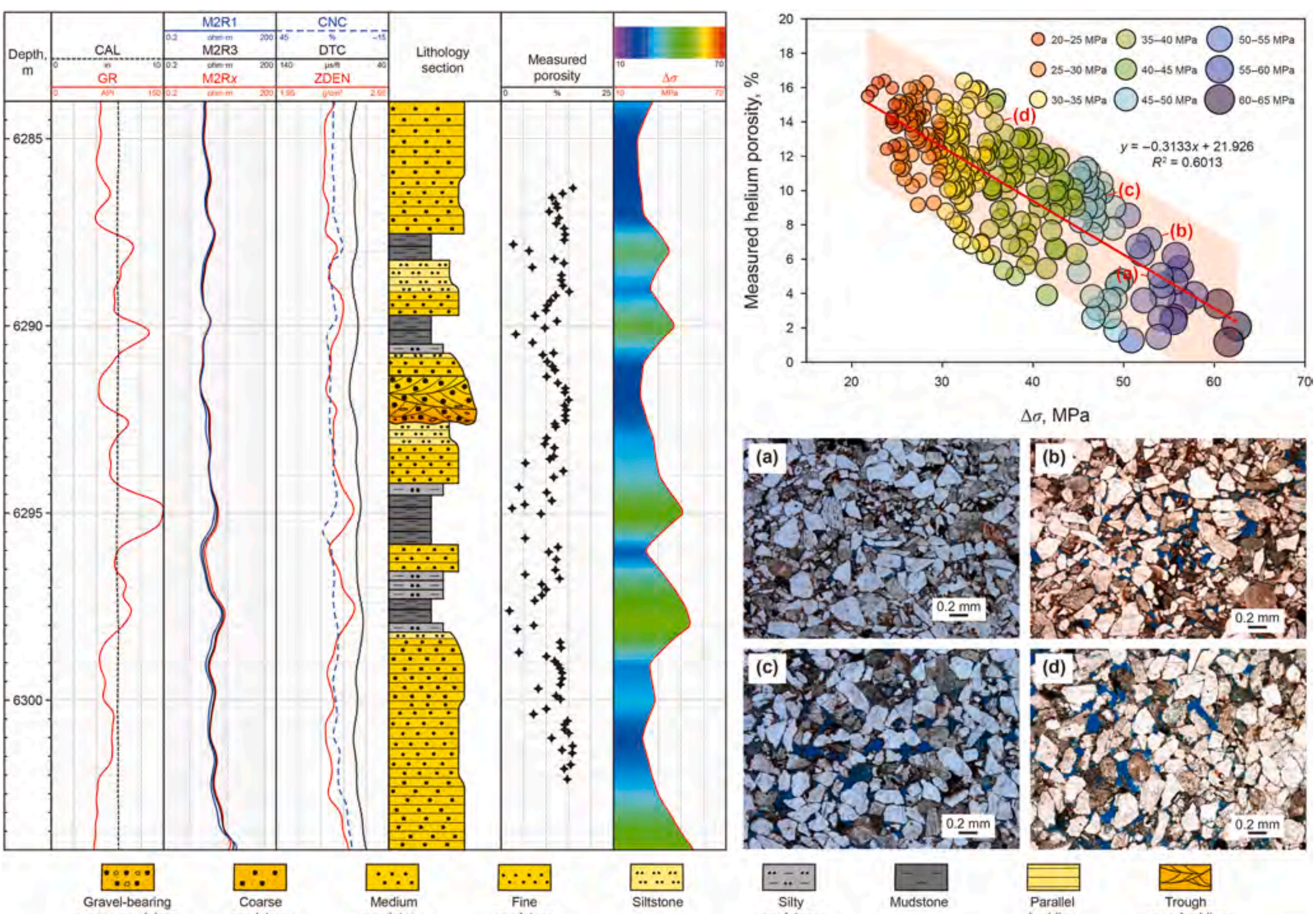

Fig. 13. Relationship between in-situ stress and porosity of Bashijiqike Formation in the Zhongqiu 1 gas field of the Kuqa Depression: **(a)** porosity = 5.06%, $\Delta\sigma$ = 54.05 MPa, Well ZQ102, 6394.25 m; **(b)** porosity = 7.12%, $\Delta\sigma$ = 52.82 MPa, Well ZQ102, 6213.12 m; **(c)** porosity = 9.53%, $\Delta\sigma$ = 46.78 MPa, Well ZQ102, 6219.43 m; **(d)** porosity = 13.97%, $\Delta\sigma$ = 35.67 MPa, Well ZQ101, 6294.79 m.

Different depositional environments have differences in composition and texture, both of which control the value of initial intergranular volume (IGV). Therefore, the pores in the center part of the underwater distributary channel sandbody can be well preserved (Fig. 10(c) and (d), 11(a)–(c)) (Taylor et al., 2010; Nguyen et al., 2013; Li et al., 2025).

5.2. Stress driven compaction and porosity loss

Stress may induce lateral and vertical compression, and lateral compression is mainly caused by horizontal compaction, and high $\Delta\sigma$ values imply a high lateral compression degree.

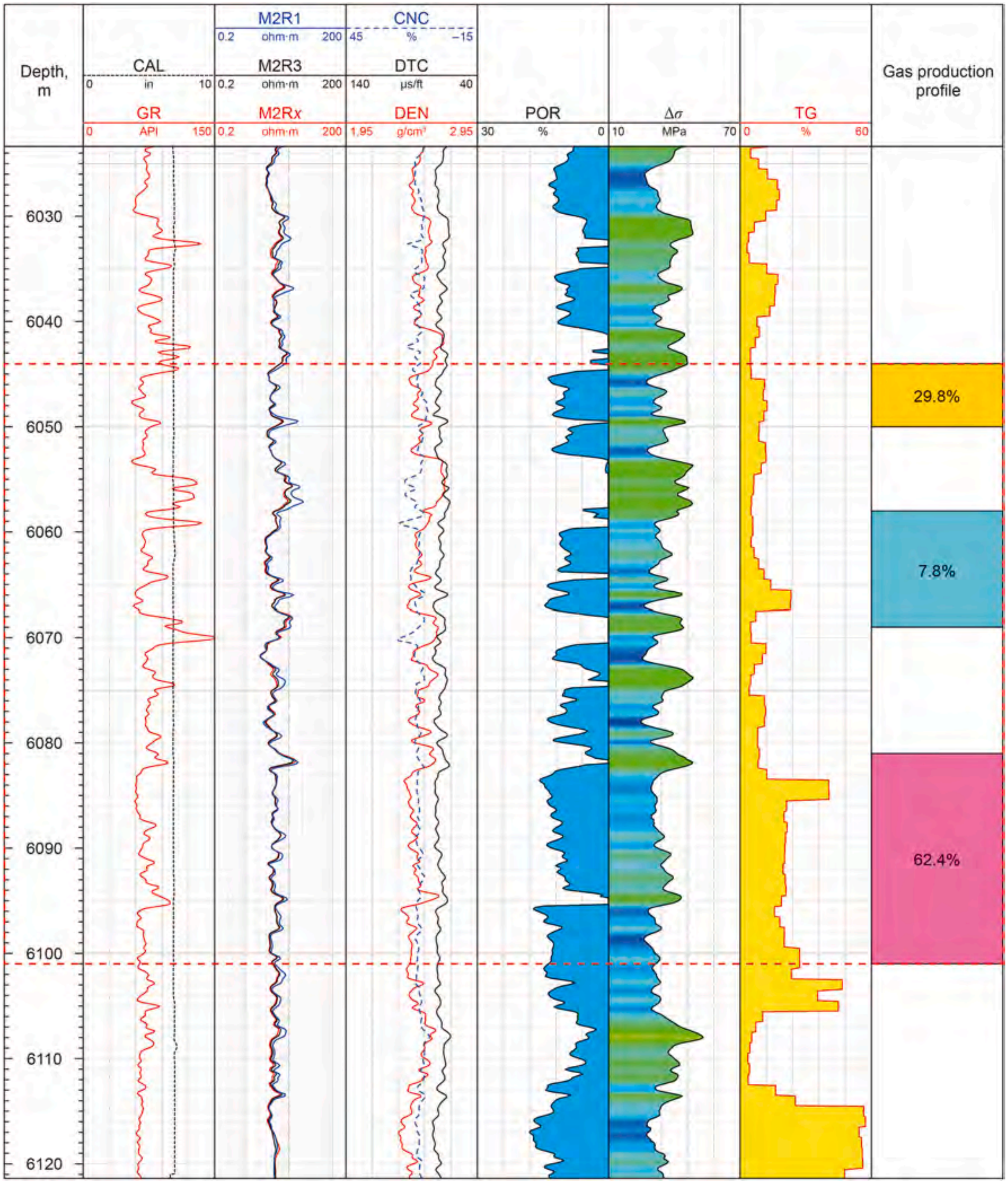

Fig. 14. Relationship between in-situ stress and gas well production for Well ZQ104 from 6044 m to 6101 m of Bashijiqike Formation in the Zhongqiu 1 gas field of the Kuqa Depression.

The compactional porosity loss (COPL) can be used to indicate the decreased porosity of the reservoir after compaction (Houseknecht, 1987; Lai et al., 2015). Additionally, the COPL is conventionally calculated by Eq. (11):

$$\mathrm{COPL} = \mathrm{OP} - \frac{\mathrm{IGV}(100 - \mathrm{OP})}{100 - \mathrm{IGV}} \tag{11}$$

where, IGV represents the sum of present intergranular porosity and cement content (intergranular porosity after compaction but before cementation); and OP represents the original porosity (Ozkan et al., 2011; Lai et al., 2022, 2023; Civitelli and Critelli, 2024; Liu et al., 2024; Guo et al., 2025).

The calculated results of Fig. 12(a) manifest that COPL shows a positive relationship with the increasing $\Delta\sigma$ values. Intensive stress will contribute to a high COPL, and COPL reaches 34.2% when the $\Delta\sigma$ is higher than 40 MPa. Extensive stress may induce a high compaction degree, and lateral stress might reduce porosity by compaction, as shown in Fig. 12(b).

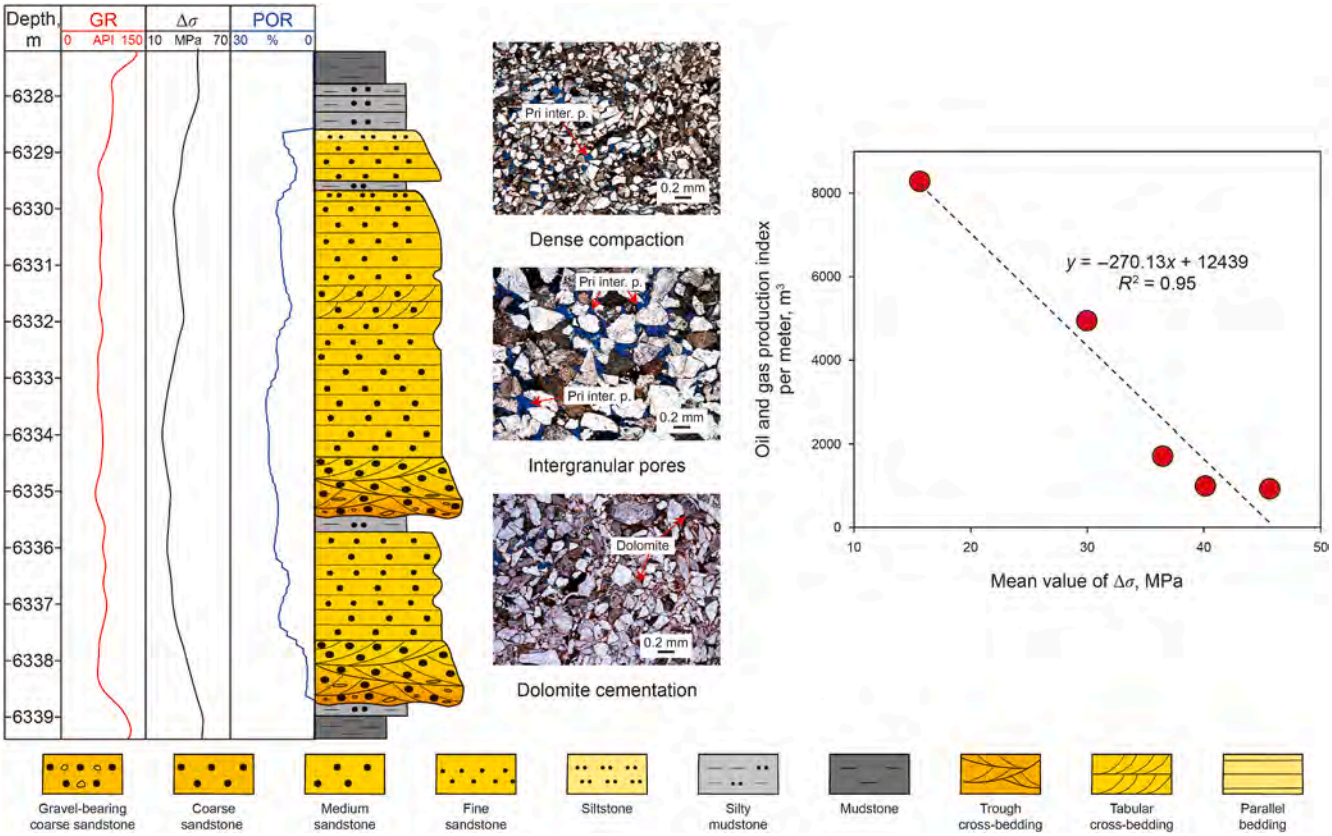

Fig. 15. Coupling relationships between hydrocarbon productivity and depositional microfacies, diagenesis and in-situ stress of Bashijiqike Formation in the Zhongqiu 1 gas field of the Kuqa Depression.

Core and thin section observations reveal that the high stress and tight compaction are mainly associated with very fine-grained or very poorly sorted sandstones (Fig. 10(a)) (Lai et al., 2023).

5.3. Impacts of in-situ stress on reservoir quality

5.3.1. In-situ stress state distribution

As previously discussed, and combined with the calculation results, the in-situ stress regime in Zhongqiu 1 gas field indicates a strike-slip stress state: $S_{\mathrm{hmax}} > S_{\mathrm{v}} > S_{\mathrm{hmin}}$ (Fig. 8).

Before stress release, elastic strain energy accumulates within the rock with minimal dissipation during the process of stress accumulation. Therefore, as stress intensifies, the rock experiences increased compression, leading to reduced porosity (Lai et al., 2022). In the Zhongqiu 1 gas field, an inverse relationship exists between $\Delta\sigma$ and core-measured porosity in the Bashijiqike Formation (Fig. 13). Additionally, the formation of natural fractures in reservoir rocks releases energy, diminishing elastic strain energy and reducing stress concentration (Faulkner et al., 2006; Xu et al., 2022b; Zhang et al., 2023; Tan et al., 2024). However, core and thin section observation from the Zhongqiu 1 gas field reveals an absence of fractures and micro-fractures in the reservoir. Consequently, it can be inferred that the in-situ stress in the Zhongqiu 1 gas field remains unreleased currently.

Moreover, lithology is a critical factor influencing the heterogeneity of in-situ stress (Li et al., 2019). Significant differences in mechanical properties (such as Young's modulus and Poisson's ratio) between sandstone and mudstone lead to distinct in-situ stress distributions within these lithologies (Yang et al., 2023). This causes abrupt changes in horizontal principal stress at sandstone-mudstone interfaces (DeReuil et al., 2019). The Bashijiqike Formation in Zhongqiu 1 gas field also consists of interbedded sandstone and mudstone sequences. Here, mudstone exhibits rheological characteristics with higher Poisson's ratios than sandstone. Calculated results in the Zhongqiu 1 gas field indicate that sandstone has greater Young's modulus values than mudstone. As a result, horizontal principal stress within mudstone layers is higher than that in sandstone (Figs. 10 and 11, 13).

5.3.2. Impact of in-situ stress on porosity

The Bashijiqike Formation reservoir in Zhongqiu 1 gas field is ultra-deeply buried and has experienced high-stress conditions, therefore in-situ stress becomes a critical factor determining reservoir quality (Lai et al., 2018b; Zivar et al., 2019). The tectonic evolution of the Qiulitage Structural Belt features early shallow burial and late rapid deep burial (Zhu et al., 2009; Lai et al., 2017b). This evolution process shortens exposure to meteoric freshwater, weakening dissolution and cementation in the Zhongqiu 1 gas field (Liu et al., 2019; Xia et al., 2025). Consequently, compaction dominates porosity reduction in the ultra-deep Bashijiqike Formation reservoir. Compaction reflects both vertical and lateral compression, and they jointly control reservoir properties (Farahani et al., 2022; Lin et al., 2023). As shown in Fig. 13, there exists an excellent negative correlation between in-situ stress magnitude and measured helium porosity.

Thin sections and cross-plot demonstrate that higher $\Delta\sigma$ value results in higher compactional porosity loss, and fewer preserved intergranular pores (Fig. 13(a)–(d)). Given the weak dissolution in Bashijiqike Formation of the Zhongqiu 1 gas field, where primary intergranular pores dominate reservoir pore spaces, and there exists a strong correlation between compaction degree and porosity, as well as between $\Delta\sigma$ and porosity. As shown in Fig. 13, the cross-plot of porosity versus $\Delta\sigma$ demonstrates that the measured helium porosity decreases with increasing $\Delta\sigma$ values. Intensive stress will result in low porosity, and the measured helium porosity is reduced to 9.4% when the $\Delta\sigma$ is higher than 40 MPa. Furthermore, the single-well plot of the Well ZQ101 indicates that $\Delta\sigma$ varies at different depths, with the measured helium porosity curve exhibiting a negative relationship with $\Delta\sigma$ curve along the vertical profile. Therefore, the higher in-situ stress magnitude, the stronger the compression and compactional porosity loss will be, and the lower the reservoir porosity.

5.3.3. *Impact of in-situ stress on gas production profile*

In theory, the presence of fluid can weaken the rock mechanical properties, including compressive strength and elastic modulus reduction, which results in effective stress decrease (Bruno and Nakagawa, 1991). This reduction mainly results from mechanical and physicochemical damages caused by reservoir pore fluids. These damages cause values of in-situ stress (calculated from well logs) to be lower in hydrocarbon-bearing intervals than in dry layers without hydrocarbons (Xu et al., 2022a). Therefore, low $\Delta\sigma$ can conversely indicate high hydrocarbon potential, which can be demonstrated in Zhongqiu 1 gas field (Fig. 14).

Fig. 14 shows that higher $\Delta\sigma$ corresponds to lower TG (total gas from gas logging curve) values. The $\Delta\sigma$ curve and the TG curve exhibits a negative correlation relationship vertically. Furthermore, the gas production profile measured from 6044 m to 6101 m confirms that low-stress intervals contribute more to gas production, while high-stress intervals contribute less (Fig. 14). The lower the in-situ stress magnitude, the higher the porosity and the better the gas producing potential.

5.4. *Reservoir quality evaluation and prediction*

The Bashijiqike Formation sandstones in Well ZQ101 primarily consist of fine- to medium-grained sandstones with well sorting and low clay content. Within the sandstone layers, particularly in the center of the sandbody, the coarser grains have a greater capability to resist compaction (Fig. 10(c) and (d)). The center part is distant from the sand-mudstone interface, and cementation is less likely to occur (Fig. 10(c) and (d)). The $\Delta\sigma$ of the Bashijiqike Formation in Well ZQ101 ranges from 18.07 MPa to 54.12 MPa, with an average of 32.15 MPa (Fig. 10). This indicates relatively weak in-situ stress and consequently moderate compaction. Consequently, primary pores are more easily preserved than the top and bottom parts of sandbodies (Fig. 10(a)–(d)). The Well ZQ101 (6270.5–6290.5 m) yields 90,781 m^3/d of gas through a 5 mm choke at 35.5 MPa drawdown pressure, with an oil and gas production index of 8279.05 m^3 per meter. Therefore, the control of in-situ stress on compaction behaviors and then the matrix porosity of sandstones determines high reservoir quality in Well ZQ101.

The sandstones in Well ZQ102 primarily consist of fine-grained (finer than Well ZQ101) sandstones with moderate sorting (poorer than in Well ZQ101) and higher clay content. The $\Delta\sigma$ of the Bashijiqike Formation in Well ZQ102 ranges from 23.96 MPa to 63.18 MPa, with an average of 40.13 MPa, indicating strong in-situ stress and intense compaction, therefore primary pores are hard to be preserved. Within the sandstone layers, particularly at the center of the sandbody, primary pores can also be preserved more than in the top and bottom in the Well ZQ102 (Fig. 11(a)–(c)), but less than in Well ZQ101. The Well ZQ102 (6191–6260 m) delivered 67,106 m^3/d of gas flow through a 5 mm choke at 20.54 MPa drawdown pressure, with an oil and gas production index of 996.55 m^3 per meter. Consequently, the control of in-situ stress on compaction behaviors and then on the matrix porosity of sandstones determines the low reservoir quality in Well ZQ102.

As shown in Fig. 15, in the top parts of the sandbodies of underwater distributary channel microfacies, the sandstones mainly show a relatively high degree of compaction due to high $\Delta\sigma$ values. Additionally, the bottom parts of the underwater distributary channel sandbodies commonly contain abundant carbonate cements. The intensive compaction or the extensive carbonate cements will result in a low hydrocarbon productivity. On the contrary, sandbodies at the center of the underwater distributary channel microfacies show a low to moderate degree of compaction due to low $\Delta\sigma$ values, and the carbonate cement content is low, and they can contribute to a high hydrocarbon productivity. Moreover, $\Delta\sigma$ values exhibit a strong negative correlation with the actual production data, therefore the in-situ stress determines reservoir porosity and also the hydrocarbon production.

6. Conclusions

(1) In the ultra-deep reservoirs of Zhongqiu 1 gas field in Kuqa Depression, the in-situ stress might remain unreleased and natural fractures are scarcely developed. Low stress is favorable for the preservation of primary pores, providing spaces for hydrocarbon accumulation, and low stress may indicate high hydrocarbon potential.
(2) High-quality reservoirs tend to develop at the center of the sandbody of underwater distributary channel microfacies (fine- to medium-grained, well-sorted and clay-poor) with moderate compaction, weak cementation, and low $\Delta\sigma$ values.
(3) Strong heterogeneity of reservoirs is closely related to in-situ stress heterogeneity. Low in-situ stress difference determines compactional porosity loss and porosity, thereby controlling gas productivity in ultra-deep sandstone reservoirs.

CRediT authorship contribution statement

Lu Xiao: Writing – original draft, Methodology, Investigation. **Jin Lai:** Writing – review & editing, Methodology, Funding acquisition. **Xun Yang:** Supervision, Investigation, Data curation. **Fei Zhao:** Supervision, Methodology, Data curation. **Dong Li:** Supervision, Methodology. **Hong-Bin Li:** Supervision, Methodology. **Yong-Ping Wu:** Resources. **Bo Zhu:** Resources. **Gui-Wen Wang:** Writing – review & editing, Supervision, Resources, Methodology.

Declaration of interests

The authors declare that they have no known competing financial interests or personal relationships that could have appeared to influence the work reported in this paper.

Acknowledgements

We thank the editor and anonymous reviewers, whose edits and suggestions served to improve the quality of the manuscript. This work is financially supported by National Science and Technology Major Project of China (2025ZD1402106), State Key Laboratory of Petroleum Resources and Engineering (PRE/indep-2501), and Science Foundation of China University of Petroleum, Beijing (No. 2462023QNXZ010). The authors thank PetroChina Tarim Oilfield Company for their data input to this work.

References

Akkiraju, V.V., Goswami, D., Kueck, J., et al., 2025. Determination of in-situ stress regime in the Koyna seismic zone, India from hydrofrac tests in a 3 km deep scientific borehole: Implications for reservoir triggered seismicity. Int. J. Rock Mech. Min. Sci. 195, 106273. https://doi.org/10.1016/j.ijrmms.2025.106273.

Anderson, E.M., 1951. In: The Dynamics of Faulting and Dyke Formation with Applications to Britain, second ed. Oliver and Boyd, Edinburgh.

Bell, J.S., Gough, D.I., 1979. Northeast-southwest compressive stress in Alberta evidence from oil wells. Earth Planet Sci. Lett. 45 (2), 475–482. https://doi.org/10.1016/0012-821X(79)90146-8.

Binh, N.T.T., Tokunaga, T., Son, H.P., et al., 2007. Present-day stress and pore pressure fields in the Cuu Long and Nam Con Son Basins, offshore Vietnam. Mar. Petrol. Geol. 24 (10), 607–615. https://doi.org/10.1016/j.marpetgeo.2007.04.002.

Bjørlykke, K., 1998. Clay mineral diagenesis in sedimentary basins: A key to the prediction of rock properties. Examples from the North Sea Basin. Clay Miner. 33 (1), 15–34. https://doi.org/10.1180/000985598545390.

Bjørlykke, K., 2014. Relationships between depositional environments, burial history and rock properties. Some principal aspects of diagenetic process in sedimentary basins. Sediment. Geol. 301, 1–14. https://doi.org/10.1016/j.sedgeo.2013.12.002.

Bruno, M.S., Nakagawa, F.M., 1991. Pore pressure influence on tensile fracture propagation in sedimentary rock. Int. J. Rock Mech. Min. Sci. Geomech. Abstr. 28 (4), 261–273. https://doi.org/10.1016/0148-9062(91)90593-B.

Cao, H., Zhao, Y., Chen, H.C., et al., 2025. Integrating well logs, 3D seismic, and earthquake data for comprehensive prediction of 3D in-situ stress orientations: A case study from the Weiyuan area in the Sichuan Basin, China. Pet. Sci. 22 (1), 210–221. https://doi.org/10.1016/j.petsci.2024.07.015.

Civitelli, M., Critelli, S., 2024. The interplay of detrital modes and depositional facies on diagenesis and petrophysics of deep-marine Miocene sandstones (Cilento Group), Southern Apennines, Italy. Mar. Petrol. Geol. 167, 106943. https://doi.org/10.1016/j.marpetgeo.2024.106943.

de Souza Rodrigues, R., Alves da Silva, F.C., Córdoba, V.C., 2021. Evolution of deformation bands, insights from structural diagenesis. J. Struct. Geol. 143, 104257. https://doi.org/10.1016/j.jsg.2020.104257.

Del Sole, L., Antonellini, M., Soliva, R., et al., 2020. Structural control on fluid flow and shallow diagenesis: Insights from calcite cementation along deformation bands in porous sandstones. Solid Earth 11 (6), 2169–2195. https://doi.org/10.5194/se-11-2169-2020.

DeReuil, A.A., Birgenheier, L.P., McLennan, J., 2019. Effects of anisotropy and saturation on geomechanical behavior of mudstone. J. Geophys. Res. Solid Earth 124 (8), 8101–8126. https://doi.org/10.1029/2018JB017034.

Dutton, S.P., 2008. Calcite cement in Permian deep-water sandstones, Delaware Basin, west Texas: Origin, distribution, and effect on reservoir properties. AAPG Bull. 92 (6), 765–787. https://doi.org/10.1306/01280807107.

Eaton, B.A., 1969. Fracture gradient prediction and its application in oilfield operations. J. Petrol. Technol. 21 (10), 1353–1360. https://doi.org/10.2118/2163-PA.

Farahani, M., Aghaei, H., Masoumi, H., 2022. Effect of pore type on porosity, permeability and pore volume compressibility of geological formations due to in-situ stress change. J. Petrol. Sci. Eng. 218, 110986. https://doi.org/10.1016/j.petrol.2022.110986.

Faulkner, D.R., Mitchell, T.M., Healy, D., et al., 2006. Slip on 'weak' faults by the rotation of regional stress in the fracture damage zone. Nature 444 (7121), 922–925. https://doi.org/10.1038/nature05353.

Feng, J.W., Ren, Q.Q., Xu, K., 2018. Quantitative prediction of fracture distribution using geomechanical method within Kuqa Depression, Tarim Basin, NW China. J. Petrol. Sci. Eng. 162, 22–34. https://doi.org/10.1016/j.petrol.2017.12.006.

Fernández-Ibáñez, F., DeGraff, J.M., Ibrayev, F., 2018. Integrating borehole image logs with core: A method to enhance subsurface fracture characterization. AAPG Bull. 102 (6), 1067–1090. https://doi.org/10.1306/0726171609317002.

Ferraro, F., Agosta, F., Ukar, E., et al., 2019. Structural diagenesis of carbonate fault rocks exhumed from shallow crustal depths: An example from the central-southern Apennines, Italy. J. Struct. Geol. 122, 58–80. https://doi.org/10.1016/j.jsg.2019.02.008.

Guo, X., Hua, Y., Wang, B., et al., 2025. Porosity evolution of sandstone reservoirs in the Paleogene Shahejie Formation of the Zhanhua depression, Bohai Bay Basin. AAPG Bull. 109 (7), 901–929. https://doi.org/10.1306/06132522006.

Guo, X.S., Hu, D.F., Li, Y.P., et al., 2019. Theoretical progress and key technologies of onshore ultra-deep oil/gas exploration. Engineering 5 (3), 458–470. https://doi.org/10.1016/j.eng.2019.01.012.

Haile, B.G., Klausen, T.G., Czarniecka, U., et al., 2018. How are diagenesis and reservoir quality linked to depositional facies? A deltaic succession, Edgeøya, Svalbard. Mar. Petrol. Geol. 92, 519–546. https://doi.org/10.1016/j.marpetgeo.2017.11.019.

Heidbach, O., Tingay, M., Barth, A., et al., 2010. Global crustal stress pattern based on the World Stress Map database release 2008. Tectonophysics 482 (1–4), 3–15. https://doi.org/10.1016/j.tecto.2009.07.023.

Houseknecht, D.W., 1987. Assessing the relative importance of compaction processes and cementation to reduction of porosity in sandstones. AAPG Bull. 71 (6), 633–642. https://doi.org/10.1306/9488787F-1704-11D7-8645000102C1865D.

Huang, S.Y., Lin, C.M., Zhang, X., et al., 2021. Controls of diagenesis on the quality of shallowly buried terrestrial coarse-grained clastic reservoirs: A case study of the Eocene Shahejie Formation in the Damintun Sag, Bohai Bay Basin, Eastern China. J. Asian Earth Sci. 221, 104950. https://doi.org/10.1016/j.jseaes.2021.104950.

Huang, Y.Y., Wang, G.W., Kuang, L.C., et al., 2025. Recognition and impact on reservoir quality of fractures in fine-grained sedimentary rocks using image and array acoustic logs. Mar. Petrol. Geol. 173, 107284. https://doi.org/10.1016/j.marpetgeo.2025.107284.

Huffman, K.A., Saffer, D.M., 2016. In situ stress magnitudes at the toe of the Nankai Trough Accretionary Prism, offshore Shikoku Island, Japan. J. Geophys. Res. Solid Earth 121 (2), 1202–1217. https://doi.org/10.1002/2015JB012415.

Ju, W., Shen, J., Qin, Y., et al., 2017. In-situ stress state in the Linxing region, eastern Ordos Basin, China: Implications for unconventional gas exploration and production. Mar. Petrol. Geol. 86, 66–78. https://doi.org/10.1016/j.marpetgeo.2017.05.026.

Ju, W., Wang, K., 2018. A preliminary study of the present-day in-situ stress state in the Ahe tight gas reservoir, Dibei Gasfield, Kuqa Depression. Mar. Petrol. Geol. 96, 154–165. https://doi.org/10.1016/j.marpetgeo.2018.05.036.

Kidambi, T., Kumar, G.S., 2016. Mechanical Earth modeling for a vertical well drilled in a naturally fractured tight carbonate gas reservoir in the Persian Gulf. J. Petrol. Sci. Eng. 141, 38–51. https://doi.org/10.1016/j.petrol.2016.01.003.

Kingdon, A., Fellgett, M.W., Williams, J.D.O., 2016. Use of borehole imaging to improve understanding of the in-situ stress orientation of Central and Northern England and its implications for unconventional hydrocarbon resources. Mar. Petrol. Geol. 73, 1–20. https://doi.org/10.1016/j.marpetgeo.2016.02.012.

Lai, J., Li, D., Ai, Y., et al., 2022. Structural diagenesis in ultra-deep tight sandstones in the Kuqa Depression, Tarim Basin, China. Solid Earth 13 (6), 975–1002. https://doi.org/10.5194/se-13-975-2022.

Lai, J., Li, D., Bai, T.Y., et al., 2023. Reservoir quality evaluation and prediction in ultra-deep tight sandstones in the Kuqa Depression, China. J. Struct. Geol. 170, 104850. https://doi.org/10.1016/j.jsg.2023.104850.

Lai, J., Li, D., Wang, G.W., et al., 2019. Earth stress and reservoir quality evaluation in high and steep structure: The Lower Cretaceous in the Kuqa Depression, Tarim Basin, China. Mar. Petrol. Geol. 101, 43–54. https://doi.org/10.1016/j.marpetgeo.2018.11.036.

Lai, J., Su, Y., Xiao, L., et al., 2024. Application of geophysical well logs in solving geologic issues: Past, present and future prospect. Geosci. Front. 15 (3), 101779. https://doi.org/10.1016/j.gsf.2024.101779.

Lai, J., Wang, G.W., Chai, Y., et al., 2015. Depositional and diagenetic controls on pore structure of tight gas sandstone reservoirs: Evidence from Lower Cretaceous Bashijiqike Formation in Kelasu thrust belts, Kuqa Depression in Tarim Basin of West China. Resour. Geol. 65 (2), 55–75. https://doi.org/10.1111/rge.12061.

Lai, J., Wang, G.W., Chai, Y., et al., 2017b. Deep burial diagenesis and reservoir quality evolution of high-temperature, high-pressure sandstones: Examples from Lower Cretaceous Bashijiqike Formation in Keshen area, Kuqa Depression, Tarim Basin of China. AAPG Bull. 101 (6), 829–862. https://doi.org/10.1306/08231614008.

Lai, J., Wang, G.W., Fan, Z.Y., et al., 2017a. Fracture detection in oil-based drilling mud using a combination of borehole image and sonic logs. Mar. Petrol. Geol. 84, 195–214. https://doi.org/10.1016/j.marpetgeo.2017.03.035.

Lai, J., Wang, G.W., Wang, S., et al., 2018a. Review of diagenetic facies in tight sandstones: diagenesis, diagenetic minerals, and prediction via well logs. Earth Sci. Rev. 185, 234–258. https://doi.org/10.1016/j.earscirev.2018.06.009.

Lai, J., Wang, G.W., Wang, S., et al., 2018b. A review on the applications of image logs in structural analysis and sedimentary characterization. Mar. Petrol. Geol. 95, 139–166. https://doi.org/10.1016/j.marpetgeo.2018.04.020.

Lai, J., Xiao, L., Song, X.Y., et al., 2026. Mechanism of reservoir property variations in deep and ultra-deep sandstones in the Kuqa Depression, China. J. Asian Earth Sci. 309, 107150. https://doi.org/10.1016/j.jseaes.2026.107150.

Laubach, S.E., Zeng, L., Hooker, J.N., et al., 2023. Deep and ultra-deep basin brittle deformation with focus on China. J. Struct. Geol. 175, 104938. https://doi.org/10.1016/j.jsg.2023.104938.

Li, D., Wang, G.W., Bie, K., et al., 2025. Formation mechanism and reservoir quality evaluation in tight sandstones under a compressional tectonic setting: The Jurassic Ahe Formation in Kuqa Depression, Tarim Basin, China. Pet. Sci. 22 (3), 998–1020. https://doi.org/10.1016/j.petsci.2024.12.026.

Li, J., Li, J., Xie, Z.Y., et al., 2020. Oil and gas source and accumulation of Zhongqiu 1 trap in Qiulitage structural belt, Tarim Basin, NW China. Petrol. Explor. Dev. 47 (3), 548–559. https://doi.org/10.1016/S1876-3804(20)60072-6.

Li, Y.X., Shen, J.S., Cai, W.Y., et al., 2022. Fractured formation evaluation by seismic attenuation derived from array acoustic log waves based on modified spectral ratio method and an extended Biot's poroelastic model. J. Petrol. Sci. Eng. 209, 109838. https://doi.org/10.1016/j.petrol.2021.109838.

Li, Z.P., Liu, X.T., Yang, Y., et al., 2019. Influences of lithology on in-situ stress field in low permeability reservoirs in Bonan Oilfield, Bohai Bay Basin, China. Petrol. Explor. Dev. 46 (4), 729–738. https://doi.org/10.1016/S1876-3804(19)60230-2.

Lin, Y., Qin, Y., Ma, D., et al., 2023. In situ stress variation and coal reservoir permeability response of the Jurassic Yan'an Formation in the southwestern Ordos Basin, China: Its impact on coalbed methane development. Geoenergy Sci. Eng. 222, 211444. https://doi.org/10.1016/j.geoen.2023.211444.

Liu, C., Xu, Z.P., Chen, G., et al., 2019. Hydrocarbon accumulation conditions and evolution process of the ZQ1 large condensate gas reservoir in the Qiulitage structural belt, Tarim Basin. Nat. Gas. Ind. 39 (4), 8–17. https://doi.org/10.3787/j.issn.1000-0976.2019.04.002 (in Chinese).

Liu, W., Zhu, Q., Qiao, Y., et al., 2024. Origin of authigenic quartz in organic-rich shales of the Dalong Formation (NW Middle Yangtze Basin), South China: Implications for pore network development. Energy Fuel. 38 (8), 6912–6926. https://doi.org/10.1021/acs.energyfuels.4c00207.

Mafakheri Bashmagh, N., Lin, W., Radwan, A.E., et al., 2024. Comprehensive analysis of stress magnitude and orientations and natural fractures in complex structural regimes oil reservoir: Implications for tectonic and oil field development in the Zagros suture zone. Mar. Petrol. Geol. 160, 106615. https://doi.org/10.1016/j.marpetgeo.2023.106615.

Maleki, S., Moradzadeh, A., Ghavami Riabi, R., et al., 2014. Comparison of several different methods of in situ stress determination. Int. J. Rock Mech. Min. Sci. 71, 395–404. https://doi.org/10.1016/j.ijrmms.2014.07.010.

Mansurbeg, H., Morad, S., Salem, A., et al., 2008. Diagenesis and reservoir quality evolution of Palaeocene deep-water, marine sandstones, the Shetland-Faroes Basin, British continental shelf. Mar. Petrol. Geol. 25 (6), 514–543. https://doi.org/10.1016/j.marpetgeo.2007.07.012.

Massiot, C., McNamara, D.D., Lewis, B., 2015. Processing and analysis of high temperature geothermal acoustic borehole image logs in the Taupo Volcanic Zone, New Zealand. Geothermics 53, 190–201. https://doi.org/10.1016/j.geothermics.2014.05.010.

Matonti, C., Guglielmi, Y., Viseur, S., et al., 2017. P-wave velocity anisotropy related to sealed fractures reactivation tracing the structural diagenesis in carbonates. Tectonophysics 705, 80–92. https://doi.org/10.1016/j.tecto.2017.03.019.

Milliken, K.L., Land, L.S., 1993. The origin and fate of silt sized carbonate in subsurface Miocene–Oligocene mudstones, south Texas Gulf Coast. Sedimentology 40 (1), 107–124. https://doi.org/10.1111/j.1365-3091.1993.tb01094.x.

Morad, S., Al-Ramadan, K., Ketzer, J.M., et al., 2010. The impact of diagenesis on the heterogeneity of sandstone reservoirs: A review of the role of depositional facies and sequence stratigraphy. AAPG Bull. 94 (8), 1267–1309. https://doi.org/10.1306/04211009178.

Najibi, A.R., Ghafoori, M., Lashkaripour, G.R., et al., 2017. Reservoir geomechanical modeling: In-situ stress, pore pressure, and mud design. J. Petrol. Sci. Eng. 151, 31–39. https://doi.org/10.1016/j.petrol.2017.01.045.

Nguyen, B.T.T., Jones, S.J., Goulty, N.R., et al., 2013. The role of fluid pressure and diagenetic cements for porosity preservation in Triassic fluvial reservoirs of the Central Graben, North Sea. AAPG Bull. 97 (8), 1273–1302. https://doi.org/10.1306/01151311163.

Nian, T., Wang, G., Xiao, C., et al., 2016. Determination of in-situ stress orientation and subsurface fracture analysis from image-core integration: An example from ultra-deep tight sandstone (BSJQK Formation) in the Kelasu Belt, Tarim Basin. J. Petrol. Sci. Eng. 147, 495–503. https://doi.org/10.1016/j.petrol.2016.09.020.

Ning, W., Ju, W., Guo, W., 2024. The present-day in-situ stress field and its effect on shale gas development in Zigong area of southern Sichuan Basin. Unconv. Resour. 4, 100078. https://doi.org/10.1016/j.uncres.2024.100078.

Ozkan, A., Cumella, S.P., Milliken, K.L., et al., 2011. Prediction of lithofacies and reservoir quality using well logs, Late Cretaceous Williams Fork Formation, Mamm Creek field, Piceance Basin, Colorado. AAPG Bull. 95 (10), 1699–1723. https://doi.org/10.1306/01191109143.

Radwan, A., Sen, S., 2021. Stress path analysis for characterization of in situ stress state and effect of reservoir depletion on present-day stress magnitudes: Reservoir geomechanical modeling in the gulf of Suez Rift Basin, Egypt. Nat. Resour. Res. 30 (1), 463–478. https://doi.org/10.1007/s11053-020-09731-2.

Rajabi, M., Sherkati, S., Bohloli, B., et al., 2010. Subsurface fracture analysis and determination of in-situ stress direction using FMI logs: An example from the Santonian carbonates (Ilam Formation) in the Abadan Plain, Iran. Tectonophysics 492 (1–4), 192–200. https://doi.org/10.1016/j.tecto.2010.06.014.

Rasouli, V., Sutherland, A., 2014. Geomechanical characteristics of gas shales: A case study in the North Perth Basin. Rock Mech. Rock Eng. 47 (6), 2031–2046. https://doi.org/10.1007/s00603-013-0531-3.

Shi, F., Liao, H., Qu, F., et al., 2024. Collaborative-driven reservoir formation pressure prediction using GAN-ML models and well logging data. Geoenergy Sci. Eng. 242, 213271. https://doi.org/10.1016/j.geoen.2024.213271.

Shi, G.R., Zhou, X.X., Zhang, G.Y., et al., 2004. The use of artificial neural network analysis and multiple regression for trap quality evaluation: A case study of the Northern Kuqa Depression of Tarim Basin in western China. Mar. Petrol. Geol. 21 (3), 411–420. https://doi.org/10.1016/j.marpetgeo.2004.01.003.

Song, I., Haimson, B.C., 1997. Polyaxial strength criteria and their use in estimating in situ stress magnitudes from borehole breakout dimensions. Int. J. Rock Mech. Min. Sci. 34 (3–4), 116.e1–116.e16. https://doi.org/10.1016/S1365-1609(97)00240-2.

Su, Y., Lai, J., Dang, W.L., et al., 2024. Pore structure characterization and reservoir quality prediction in deep and ultra-deep tight sandstones by integrating image and NMR logs. J. Asian Earth Sci. 272, 106232. https://doi.org/10.1016/j.jseaes.2024.106232.

Su, Y., Lai, J., Dang, W.L., et al., 2026. Geological factors and fracture distribution in deep and ultra-deep sandstones in Kuqa Depression, Tarim Basin, China. Solid Earth 17 (4), 643–664. https://doi.org/10.5194/se-17-643-2026.

Sun, D., Zhang, C.Y., Zhang, S.A., et al., 2025. Hydraulic fracturing in-situ stress measurements and large deformation evaluation of 1000 m-deep soft rock roadway in Jinchuan No. 2 mine, northwestern China. Rock Mech. Rock Eng. 58 (3), 2781–2801. https://doi.org/10.1007/s00603-024-04273-y.

Sun, S., Hou, G.T., Zheng, C.F., 2017. Fracture zones constrained by neutral surfaces in a fault-related fold: Insights from the Kelasu tectonic zone, Kuqa Depression. J. Struct. Geol. 104, 112–124. https://doi.org/10.1016/j.jsg.2017.10.005.

Tan, P., Chen, Z.W., Huang, L.K., et al., 2024. Evaluation of the combined influence of geological layer property and in-situ stresses on fracture height growth for layered formations. Pet. Sci. 21 (5), 3222–3236. https://doi.org/10.1016/j.petsci.2024.07.014.

Taylor, T.R., Giles, M.R., Hathon, L.A., et al., 2010. Sandstone diagenesis and reservoir quality prediction: Models, myths, and reality. AAPG Bull. 94 (8), 1093–1132. https://doi.org/10.1306/04211009123.

Teng, C., Cai, Z., Hao, F., et al., 2020. Structural geometry and evolution of an intracratonic strike-slip fault zone: A case study from the north SB5 fault zone in the Tarim Basin, China. J. Struct. Geol. 140, 104159. https://doi.org/10.1016/j.jsg.2020.104159.

Thiercelin, M.J., Plumb, R.A., 1994. Core-based prediction of lithologic stress contrasts in east Texas formations. SPE Form. Eval. 9 (4), 251–258. https://doi.org/10.2118/21847-PA.

Thyne, G., 2001. A model for diagenetic mass transfer between adjacent sandstone and shale. Mar. Petrol. Geol. 18 (6), 743–755. https://doi.org/10.1016/S0264-8172(01)00025-3.

Tian, Y., Wang, D., Xia, J., et al., 2025. Digital rock modeling of deformed multi-scale media in deep hydrocarbon reservoirs based on in-situ stress-loading CT imaging and U-Net deep learning. Mar. Petrol. Geol. 171, 107177. https://doi.org/10.1016/j.marpetgeo.2024.107177.

Tingay, M., Bentham, P., De Feyter, A., et al., 2011. Present-day stress-field rotations associated with evaporites in the offshore Nile Delta. Geol. Soc. Am. Bull. 123 (5–6), 1171–1180. https://doi.org/10.1130/B30185.1.

Tingay, M.R.P., Hillis, R.R., Morley, C.K., et al., 2009. Present-day stress and neotectonics of Brunei: Implications for petroleum exploration and production. AAPG Bull. 93 (1), 75–100. https://doi.org/10.1306/08080808031.

Vandeginste, V., Swennen, R., Allaeys, M., et al., 2012. Challenges of structural diagenesis in foreland fold-and-thrust belts: A case study on paleofluid flow in the Canadian Rocky Mountains West of Calgary. Mar. Petrol. Geol. 35 (1), 235–251. https://doi.org/10.1016/j.marpetgeo.2012.02.014.

Verweij, J.M., Boxem, T.A.P., Nelskamp, S., 2016. 3D spatial variation in vertical stress in on- and offshore Netherlands; integration of density log measurements and basin modeling results. Mar. Petrol. Geol. 78, 870–882. https://doi.org/10.1016/j.marpetgeo.2016.06.016.

Wang, H., Xi, K.L., Cao, Y.C., et al., 2025. The formation mechanism of high-quality clastic rock reservoir controlled by coupling of “structure-lithofacies-fluid” in the foreland thrust belt in northern Kuqa, Tarim Basin, Northwestern China. Pet. Sci. 22 (11), 4357–4380. https://doi.org/10.1016/j.petsci.2025.08.004.

Wei, G.Q., Wang, K., Zhang, R.H., et al., 2022. Structural diagenesis and high-quality reservoir prediction of tight sandstones: A case study of the Jurassic Ahe Formation of the Dibei gas reservoir, Kuqa Depression, Tarim Basin, NW China. J. Asian Earth Sci. 239, 105399. https://doi.org/10.1016/j.jseaes.2022.105399.

Wilson, T.H., Smith, V., Brown, A., 2015. Developing a model discrete fracture network, drilling, and enhanced oil recovery strategy in an unconventional naturally fractured reservoir using integrated field, image log, and three-dimensional seismic data. AAPG Bull. 99 (4), 735–762. https://doi.org/10.1306/10031414015.

Xia, W.H., Yin, J.Y., He, Z.Y., et al., 2025. Meso-Cenozoic tectonic and thermal history of the Kuqa Depression, Tarim Basin: Insights from low-temperature thermochronology and vitrinite reflectance. J. Earth Sci. 36 (3), 1290–1296. https://doi.org/10.1007/s12583-025-2027-y.

Xiang, M., Wang, Z.W., Liu, J.H., 2015. Extracting array acoustic logging signal information by combining fractional Fourier transform and Choi–Williams distribution. Appl. Acoust. 90, 111–115. https://doi.org/10.1016/j.apacoust.2014.11.004.

Xu, K., Tian, J., Yang, H.J., et al., 2022b. Effects and practical applications of present-day in-situ stress on reservoir quality in ultra-deep layers of Kuqa Depression, Tarim Basin, China. J. Nat. Gas Geosci. 7 (2), 85–94. https://doi.org/10.1016/j.jnggs.2022.04.002.

Xu, K., Yang, H.J., Zhang, H., et al., 2022a. Fracture effectiveness evaluation in ultra-deep reservoirs based on geomechanical method, Kuqa Depression, Tarim Basin, NW China. J. Petrol. Sci. Eng. 215, 110604. https://doi.org/10.1016/j.petrol.2022.110604.

Xu, X.T., Zeng, L.B., Dong, S.Q., et al., 2025. The characteristics and controlling factors of high-quality reservoirs of ultra-deep tight sandstone: A case study of the Dabei Gas Field, Tarim Basin, China. Pet. Sci. 22 (9), 3473–3496. https://doi.org/10.1016/j.petsci.2025.03.033.

Yang, R.Y., Cong, R.C., Gong, Y.J., et al., 2023. Micromechanical contrast of Ordos Basin sandstone-mudstone interbedded layered rocks. J. Geophys. Res. Solid Earth 128 (10). https://doi.org/10.1029/2023JB027190 e2023JB027190.

Yeltsov, I.N., Nazarova, L.A., Nazarov, L.A., et al., 2014. Geomechanics and fluid flow effects on electric well logs: Multiphysics modeling. Russ. Geol. Geophys. 55 (5–6), 775–783. https://doi.org/10.1016/j.rgg.2014.05.020.

Zeng, L.B., Liu, G.P., Zhu, R.K., et al., 2020a. A quantitative evaluation method of structural diagenetic strength of deep tight sandstone reservoirs in Kuqa foreland basin. Acta Pet. Sin. 41 (12), 1601–1609. https://doi.org/10.7623/syxb202012012 (in Chinese).

Zeng, L.B., Wang, H.J., Gong, L., et al., 2010. Impacts of the tectonic stress field on natural gas migration and accumulation: A case study of the Kuqa Depression in the Tarim Basin. China. Mar. Petrol. Geol. 27 (7), 1616–1627. https://doi.org/10.1016/j.marpetgeo.2010.04.010.

Zeng, Q.L., Mo, T., Zhao, J.L., et al., 2020b. Characteristics, genetic mechanism and oil & gas exploration significance of high-quality sandstone reservoirs deeper than 7000 m: a case study of the Bashijiqike Formation of Lower Cretaceous in

the Kuqa Depression, NW China. Nat. Gas Ind. B 7 (4), 317–327. https://doi.org/10.1016/j.ngib.2020.01.003.
Zhang, C.Y., Fan, D.J., Elsworth, D., et al., 2024a. Mechanisms of stress- and fluid-pressure-driven fault reactivation in Gonghe granite: implications for injection-induced earthquakes. Int. J. Rock Mech. Min. Sci. 174, 105642. https://doi.org/10.1016/j.ijrmms.2024.105642.
Zhang, C.Y., Li, B., Li, H.L., et al., 2023. Stress estimation in a 3 km-deep geothermal borehole: A snapshot of stress state in Southern Cathaysia block, China. Tectonophysics 864, 230031. https://doi.org/10.1016/j.tecto.2023.230031.
Zhang, C.Y., Lin, W.R., He, M.C., et al., 2022. Determining in-situ stress state by anelastic strain recovery method beneath Xiamen: Implications for the coastal region of southeastern China. Rock Mech. Rock Eng. 55 (9), 5687–5703. https://doi.org/10.1007/s00603-022-02915-7.
Zhang, H., Zhang, G.J., Xu, K., et al., 2024b. Characteristics of stress state transitions and its geological and mechanical response in the Kuqa Depression. Earth Sci. Front. 31 (5), 177–194. https://doi.org/10.13745/j.esf.sf.2023.6.25 (in Chinese).
Zhang, J.C., 2011. Pore pressure prediction from well logs: Methods, modifications, and new approaches. Earth Sci. Rev. 108 (1–2), 50–63. https://doi.org/10.1016/j.earscirev.2011.06.001.
Zhang, K.P., Chen, M., Zhao, C.J., et al., 2024c. A continuous and long-term in-situ stress measuring method based on fiber optic. Part I: theory of inverse differential strain analysis. Pet. Sci. 21 (2), 1171–1189. https://doi.org/10.1016/j.petsci.2023.10.006.
Zhang, Y., Zhang, J., 2017. Lithology-dependent minimum horizontal stress and in-situ stress estimate. Tectonophysics 703–704, 1–8. https://doi.org/10.1016/j.tecto.2017.03.002.
Zhao, F., Lai, J., Xia, Z.L., et al., 2025. Coaly source rock evaluation using well logs: The Jurassic Kezilenuer Formation in Kuqa Depression, Tarim Basin, China. Pet. Sci. 22 (9), 3599–3612. https://doi.org/10.1016/j.petsci.2025.05.029.
Zhu, G.Y., Zhang, S.C., Chen, L., et al., 2009. Coupling relationship between natural gas charging and deep sandstone reservoir formation: A case from the Kuqa Depression, Tarim Basin. Petrol. Explor. Dev. 36 (3), 347–357. https://doi.org/10.1016/S1876-3804(09)60132-4.
Zhu, S.B., Du, Q.W., Dong, C., et al., 2023. Reservoir characteristics and controlling factors of large-scale mono-block gas field developed in delta-front sandstone: A case study from Zhongqiu 1 gas field in the Tarim Basin. Minerals 13 (10), 1326. https://doi.org/10.3390/min13101326.
Zivar, D., Foroozesh, J., Pourafshary, P., et al., 2019. Stress dependency of permeability, porosity and flow channels in anhydrite and carbonate rocks. J. Nat. Gas Sci. Eng. 70, 102949. https://doi.org/10.1016/j.jngse.2019.102949.
Zoback, M.D., Apel, R., Baumgärtner, J., et al., 1993. Upper-crustal strength inferred from stress measurements to 6 km depth in the KTB borehole. Nature 365 (6447), 633–635. https://doi.org/10.1038/365633a0.
Zoback, M.D., Barton, C.A., Brudy, M., et al., 2003. Determination of stress orientation and magnitude in deep wells. Int. J. Rock Mech. Min. Sci. 40 (7–8), 1049–1076. https://doi.org/10.1016/j.ijrmms.2003.07.001.